GFZ

Helmholtz-Zentrum
POTSDAM

HELMHOLTZ-ZENTRUM POTSDAM
DEUTSCHES
GEOFORSCHUNGSZENTRUM

G. Grünthal, A. Hakimhashemi, H. Schelle,
Ch. Bosse, R. Wahlström

The long-term temporal behaviour of the seismicity of the Dead Sea Fault Zone and its implication for time-dependent seismic hazard assessments

Scientific Technical Report STR09/09

www.gfz-potsdam.de

HELMHOLTZ
GEMEINSCHAFT

Deutsches GeoForschungsZentrum GFZ
Scientific Technical Report 09/09
DOI:10.2312/GFZ.b103-09098

Impressum

Helmholtz-Zentrum Potsdam
Deutsches GeoForschungsZentrum
Telegrafenberg
D-14473 Potsdam

Gedruckt in Potsdam
Dezember 2009

ISSN 1610-0956

Die vorliegende Arbeit
in der Schriftenreihe
Scientific Technical Report (STR) des GFZ
ist in elektronischer Form erhältlich unter
www.gfz-potsdam.de
Neuestes - Neue Publikationen des GFZ

Deutsches GeoForschungsZentrum GFZ
Scientific Technical Report 09/09
DOI:10.2312/GFZ.b103-09098

G. Grünthal, A. Hakimhashemi, H. Schelle, Ch. Bosse, R. Wahlström

The long-term temporal behaviour of the seismicity of the Dead Sea Fault Zone and its implication for time-dependent seismic hazard assessments

A report related to the DFG project Geo-DESIRE (Geoscientific Dead Sea Integrated Research Project), with participating institutions from Germany, Israel, Jordan and Palestine territories.

Scientific Technical Report STR09/09

Deutsches GeoForschungsZentrum GFZ
Scientific Technical Report 09/09
DOI:10.2312/GFZ.b103-09098

Deutsches GeoForschungsZentrum GFZ
Scientific Technical Report 09/09
DOI:10.2312/GFZ.b103-09098

Contents

Deutsches GeoForschungsZentrum GFZ
Scientific Technical Report 09/09
DOI:10.2312/GFZ.b103-09098

1. Introduction

The active boundary between the Anatolian plate and the African plate follows the Red Sea, splays south of Sinai into the Gulf of Suez and the Gulf of Aqaba and continues onshore as the Dead Sea fault zone (DSFZ). During the very long lasting history of the area crossed by the DSFZ, which extends to several millennia, repeatedly devastating earthquakes have occurred. This means that the area is exposed to a relatively high seismic hazard and also to a high seismic risk in population centres and industrial agglomerations. However, during the last almost two centuries strong earthquakes are lacking there, except the $M_w = 7.3$ earthquake in 1995 in the Gulf of Aqaba, which makes the area especially insidious. The second last $M_w > 6.5$ event along the DSFZ occurred in 1872. The well-known so-called Jericho earthquake in 1927 had an $M_w \approx 6.1$ according to recent studies (*Avni et al.*, 2002). The seismic awareness has increased after the last, strongly felt earthquake in the area of the Dead Sea basin 2004 with $M_w = 5.3$ (*Al-Tarazi et al.*, 2006).

Consequently, this area has been subject to probabilistic seismic hazard assessment (PSHA). We want to mention, as examples, *Al-Tarazi & Sandvol* (2007), *Abdallah et al.* (2006), *Jiménez et al.* (2006), *Elnashai & El-Khoury* (2004), *Harajli et al.* (2002), Mayer-Rosa & Selami (as part of *Grünthal et al.* 1999), *Husein Malkawi et al.* (1995), and *Arieh & Rabinowitz* (1989).

The seismicity of the area along the DSFZ shows in a long-term view a remarkable feature: Periods of high seismic activities are followed by periods where strong earthquakes are lacking. The periods of high activity seem to be much shorter than those of quiescence. This characteristic behaviour can be deduced from seismicity or stress transfer studies for this area, where we want to mention *Sieberg* (1932a) as one of the earliest and *Heidbach & Ben-Avraham* (2007) as one of the current ones. Actually, such a strong time dependence in seismic activity should, consequently, result in also time-dependent PSHA. The intuitive impression of time dependence has to be subject to rigorous statistical tests.

The paper consists of two main elements: (1) the creation of a harmonized seismicity data file for the eastern Mediterranean area and the generation of a classical time-independent PSHA, and (2) the extension of the earthquake model of the time-independent approach to a newly developed time-dependent PSHA and the comparison with the results of (1).

2. Generation of a harmonized seismicity data file for the eastern Mediterranean area

There exists a considerable number of earthquake catalogues and seismicity data files for at least parts of the eastern Mediterranean area. However, hardly any of them have a sufficient spatial and temporal coverage including sufficiently low magnitude

Deutsches GeoForschungsZentrum GFZ
Scientific Technical Report 09/09
DOI:10.2312/GFZ.b103-09098

thresholds. *Ambraseys et al.* (2002) reviewed the regional catalogues (both historical and instrumental) of eastern Mediterranean and Middle East and concluded that all of them have deficiencies with respect to the quality of the parameterization. Therefore, such a data file had to be generated first. We follow here the methodology developed and described for the central, northern and northwestern European earthquake catalogue CENEC (*Grünthal et al.* 2009a) whose extension to the south (EMEC – the Euro-Mediterranean earthquake catalogue) is briefly laid out in *Grünthal & Wahlström* (2009). Basically the data in three of the areal polygons derived for EMEC are required for this study, the SE Mediterranean area, Turkey (eastern part), and Cyprus including its adjacent off-shore areas. A list of the priorities for catalogue selection in the polygons for various time periods is given in Table 1.

Table 1. Catalogues, data files and their hierarchies in the polygons SE Mediterranean area, Turkey and Cyprus for different time periods. References: **AA** *Ambraseys and Adams* (1993); **AFS** *Abdallah et al.* (2004); **AMA** *Ambraseys et al.* (1994); **FA** *Feldman & Amrat* (2007); **GC** *Guidoboni & Comastri* (2005); **GD** *Galanopoulos & Delibasis* (1965); **Kan** *Kandilli Observatory* (2009); **KKP** *Khair et al.* (2000); **SDM** *Sbeinati et al.* (2005); **Pap** *Papazachos et al.* (2003); **Tar** *Al-Tarazi* (2002), **TR-GSHAP** *ETH & Swiss Seismological Service* (2000). In addition, data were provided by a few special studies, notably *Ambraseys* (2006).

SE Mediterranean area; time period	Catalogue priority
-349	**SDM, KKP, AMA**
350-999	**SDM, KKP, FA, AMA**
1000-1499	**SDM, KKP, GC, FA, AMA**
1500-1899	**SDM, KKP, FA, AMA**
1900-1992	**KKP, AMA, AFS, Tar, Kan**
Turkey; time period	
-349	**SDM, KKP, TR-GSHAP**
350-999	**SDM, KKP, FA, TR-GSHAP**
1000-1499	**SDM, KKP, GC, TR-GSHAP**
1500-1899	**SDM, TR-GSHAP**
1900-1999	**KKP, Pap, Kan**
Cyprus; time period	
-999	**GD**
1000-1499	**GC, FA, GD**
1500-1889	**FA, GD**
1890-1899	**AA, FA**
1900-1963	**AA, AFS, Kan, GD**

3. Seismicity and tectonic setting

The epicentres of the selected seismicity data file are shown in Figure 1a. The data have been depicted since 300 AD. The increased seismicity along the DSFZ is obvious. Its southern extension, running through the Gulf of Aqaba, shows the dense distribution of epicentres which mostly belong to the aftershock series of the strong 1995

Deutsches GeoForschungsZentrum GFZ
Scientific Technical Report 09/09
DOI:10.2312/GFZ.b103-09098

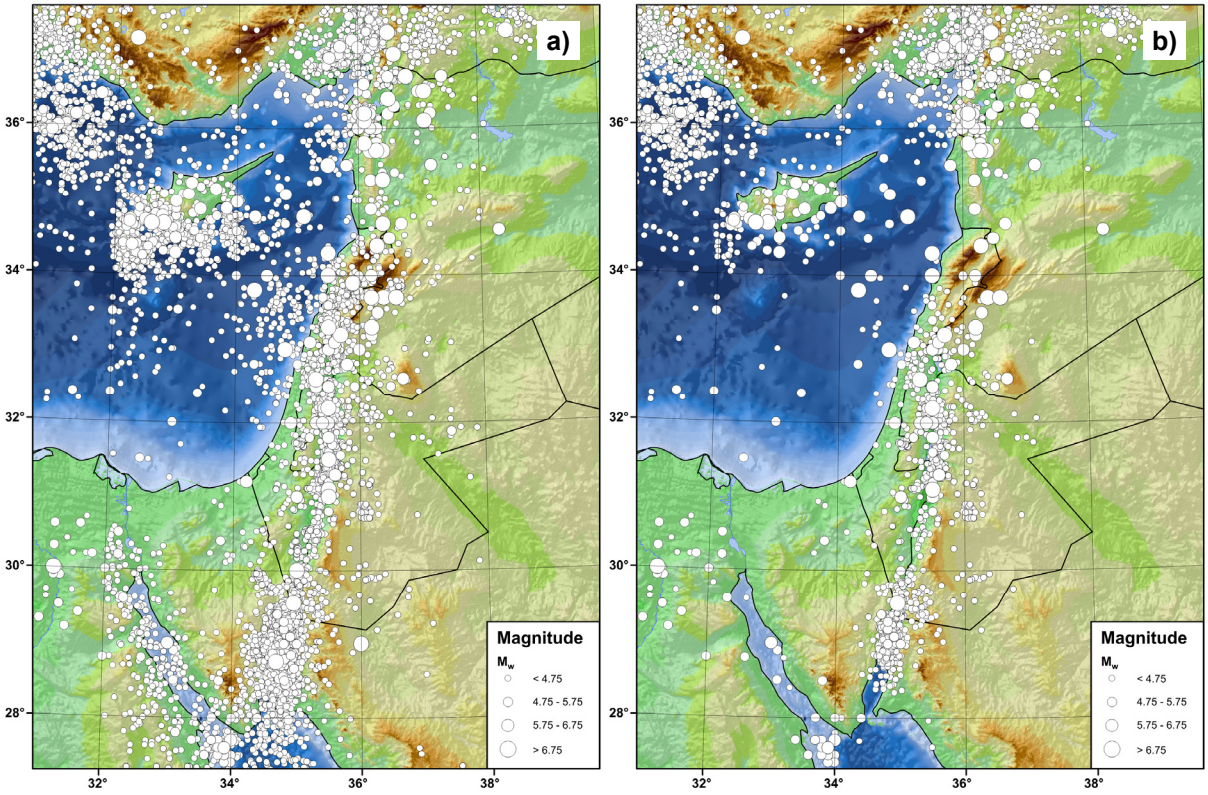

Figure 1. Seismicity of the study area according to the EMEC data file in its version from 2009. **a)** All catalogued events; one of the data files of the Levant, i.e. *Abdallah et al.* (2004), extends westwards up to 32°E only, which can be well seen in the map. **b)** The data set without the *Abdallah et al.* (2004) data file, which is less complete but gives an unbiased view on the seismicity of the area W and E of 32°E.

earthquake with $M_w = 7.3$ after *Klinger et al.* (1999) or $M_w = 7.2$ after *Hofstetter* (2003). Also the Gulf of Suez is seismically active.

The sharp cut of seismicity at 32°E to be seen especially clearly SW of Cyprus and in Egypt with definitely less activity W of this latitude, is mainly due to the fact that the RELEMR-catalogue (*Abdallah et al.* 2004) for the 20th century (from 1900 to July 2006) does not extend W of 32°E. However, there is a need to have an unbiased seismicity distribution just around this latitude, since there one assumes the western boundary of the Sinai block as described below, although its exact position could so far not be clearly defined. Since we want to contribute to this issue, previously discussed by *Papazachos & Papaioannou* (1999) as a NNE striking transform dextral fault (the Paphos transform fault PTF) which connects, with the help of the spatial distribution of the newly compiled seismicity data, an epicentre map is needed which shows homogeneous seismicity around 32°E. In Figure 1b the epicentres are shown therefore without the RELEMR-catalogue. Of course, this figure provides a much less complete view of the seismicity with respect to small magnitude events, but it gives an unbiased picture around 32°E. We can see now that the seismicity SW of Cyprus does not end sharply at 32°E but along a NNE-SSW directed strike immediately E of 32°E, i.e. the PTF, as described by *Papazachos & Papaioannou* (1999). The seismicity distribution (Fig. 1b) constrains a slightly "steeper" direction of the PTF than originally described. This strike is marked by

Deutsches GeoForschungsZentrum GFZ
Scientific Technical Report 09/09
DOI:10.2312/GFZ.b103-09098

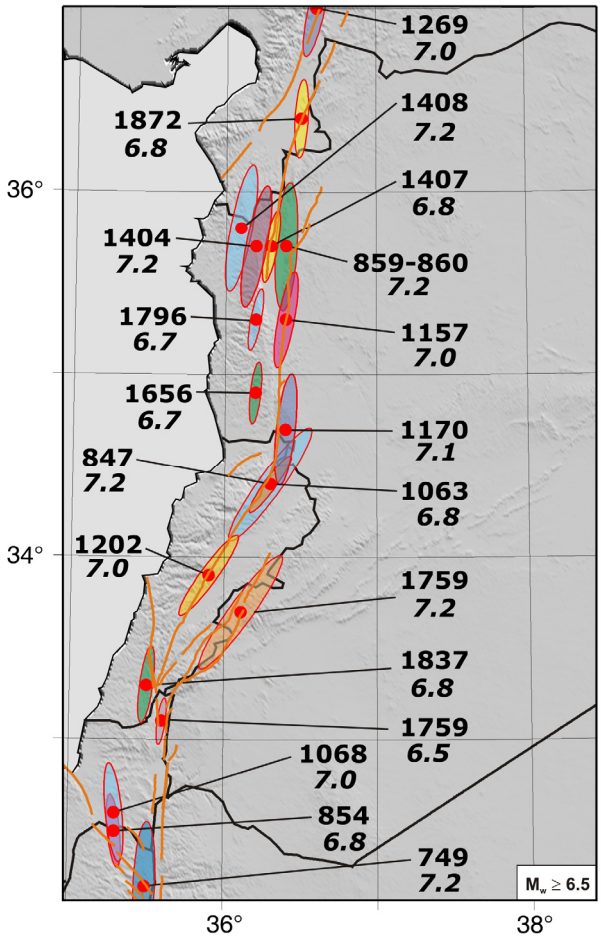

Figure 2. Seismic fault ruptures of events with $M_w \geq 6.5$ since 700 AD according to the EMEC data file. The fault lengths have been calculated according to *Wells & Coppersmith* (1994). The used colours are only to distinguish different events.

a number of significant earthquakes which recently have been recorded, e.g. $M_w = 6.4$ (1953/09/10), $M_w = 6.1$ (1995/02/23), $M_w = 6.8$ (1996/10/09), $M_w = 6.1$ (199701/13). Two significant events have been located at 32°E, half way between Cyprus and Egypt, $M_w = 4.9$ (1941/04/28) and $M_w = 5.4$ (1953/02/01). It cannot be excluded that these events might be related to the western bound of the Sinai block as it is discussed below.

Further east the seismicity of the arc extends towards the fault system which forms the seismically also very active East Anatolian fault zone (EAFZ). The Dead Sea fault zone (DSFZ) from the Sinai block triple junction within the northern part of the Red Sea in the south up to its transition in the EAFZ in the north, shows in a long term view a remarkable seismicity as well. The seismicity of the central part of the DSFZ seems to be diffusely linked with the seismically active Cyprus arc. This phenomenon cannot be explained so far by any known tectonic feature. The role of the Carmel fault, which splays off the DSFZ with a NNW strike and continues off-shore N of Haifa, is not yet understood in this respect.

Figure 2 shows the northern part of the DSFZ with probable rupture extensions due to $M_w \geq 6.5$ earthquakes since 300 AD. The lengths of the ruptured segments have been calculated by applying the empirical relation between M_w and fault area given by

Deutsches GeoForschungsZentrum GFZ
Scientific Technical Report 09/09
DOI:10.2312/GFZ.b103-09098

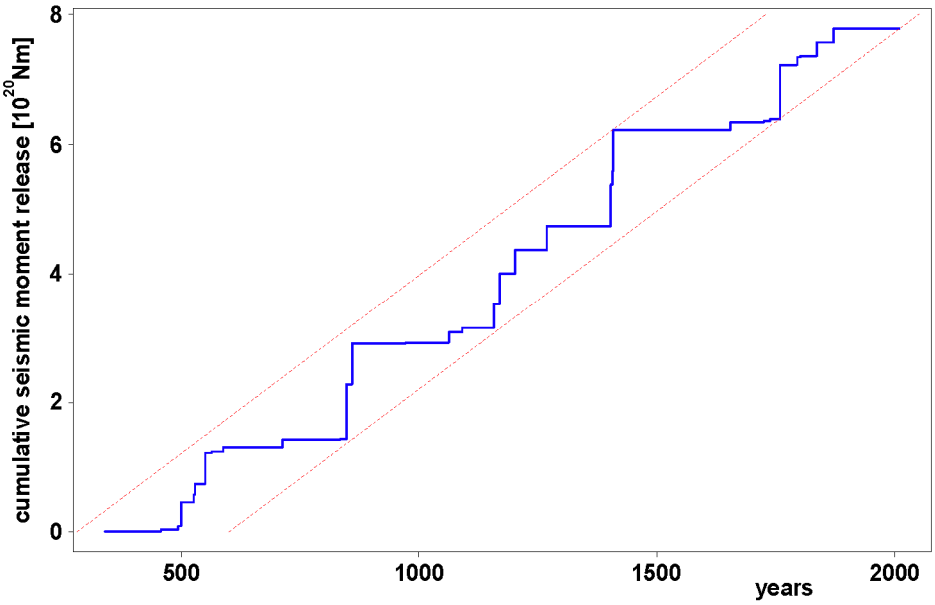

Figure 3. The cumulative seismic moment release with time (from 360 AD up to 2009) in the northern part of the DSFZ (seismic source zones YGK and Rashya), which exhibits cyclicity in seismic activity.

Wells & Coppersmith (1994) using a seismogenic depth range of 25 km. The figure reveals that most elements of the DSFZ have been affected by fault ruptures since 300 AD, but very few segments have been affected twice since that time. Although we have to assume a considerable uncertainty both in magnitude and location, the derived pattern of ruptures yields at least a reasonable picture.

The cumulative seismic moment release along the DSFZ indicates a pronounced periodic behaviour, i.e. long-time periods of relative seismic quiescence separated by high active phases. This is especially clear along the northern part of the DSFZ (Fig. 3). This periodic feature was basically the motivation for us (1) to test if the seismicity along the DSFZ requires to apply time-dependent occurrence rates of events, and, if so, (2) to use them for a time-dependent PSHA described below.

The tectonic setting of the study area is schematically depicted in Figure 4. The target area of the PSHA is the Levant, represented tectonically as the DSFZ which makes up the eastern border of the Sinai block as described, e.g. by *Mahmoud et al.* (2005). The Levant with its remarkable tectonic features has even been in the focus of geology in its very early stages. We reproduce here (Fig. 5) as an example the fault structure map by *Diener* (1886) which already reflects today's knowledge surprisingly well.

As DSFZ we understand here the entire plate boundary system delimited by the Sinai triple junction to the S and the southwesternmost part of the EAFZ to the N. The following segments of the DSFZ can be distinguished (from S to N, see Fig. 4):

- pull-apart structures of the Gulf of Aqaba,
- Wadi Arava fault,
- Dead Sea pull-apart section,
- Jordan valley,
- Hula and Lake Kinneret faults,

Deutsches GeoForschungsZentrum GFZ
Scientific Technical Report 09/09
DOI:10.2312/GFZ.b103-09098

- Yammoûneh fault,
- Ghab fault,
- Kasaru fault.

The DSFZ was formed as the result of the Cenozoic rifting between the African and Arabian plates (*Freund* 1965, *Garfunkel & Ben-Avraham* 1996). It accommodates a left-lateral displacement of in total about 105 km (*Quennel* 1959, *Freund et al.* 1970, *Bandel & Khouri* 1981).

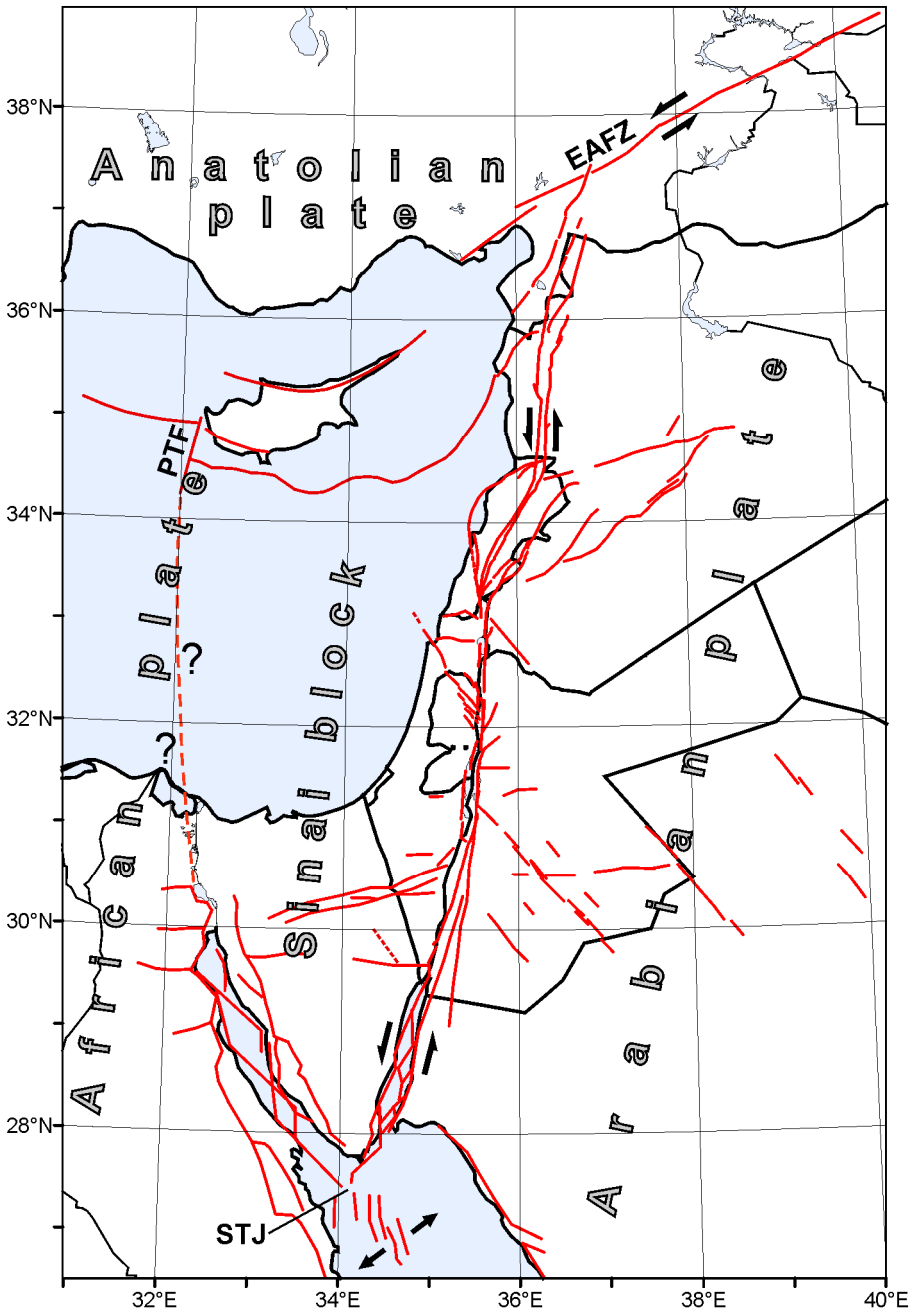

Figure 4. Tectonic setting of the Sinai block and of the Levant. The Dead Sea fault zone (DSFZ) represents the northwestern boundary between the Arabian plate and the Sinai block, ranging from the Sinai triple junction (STJ) in the S up to the East Anatolian fault zone (EAFZ) in the N. The Paphos transform fault (PTF) and the Gulf of Suez constrain the western border of the Sinai block. The Cyprean arc forms the northern border of the Sinai block. Further notations of faults or tectonic elements having relevance for the seismic hazard assessment are given in Fig. 7b.

Deutsches GeoForschungsZentrum GFZ
Scientific Technical Report 09/09
DOI:10.2312/GFZ.b103-09098

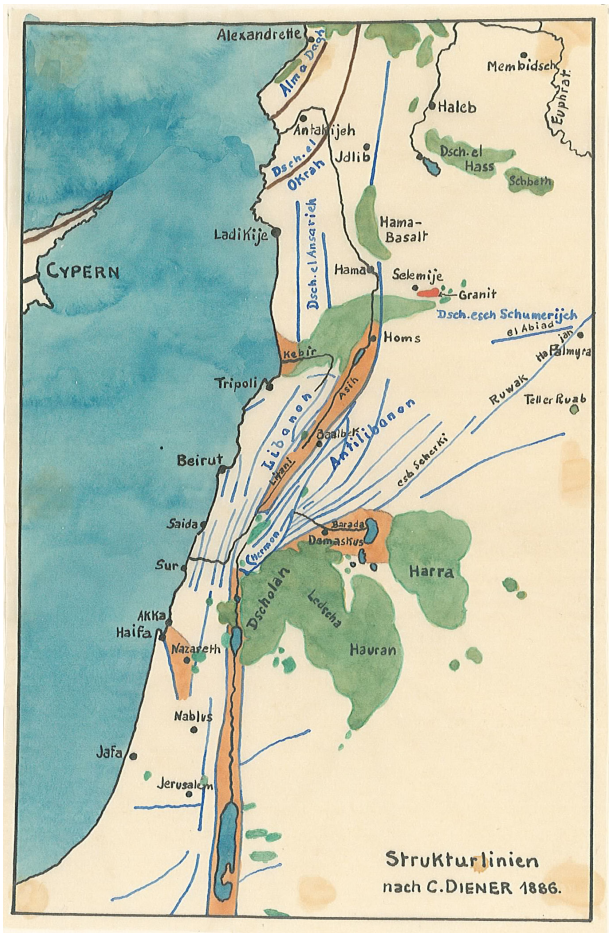

Figure 5. Structural lines (in blue) of the central part of the DSFZ by *Diener* (1886); redrawing of Diener's "Übersichtskarte der Strukturlinien von Syrien" by Sieberg. Green: basalts, brown: fields of subsidence, red: granites.

The assessment of the seismic hazard for the Levant requires to consider not only the seismicity of the DSFZ but also that of the entire Sinai block, whose SE and SW bounds represent the Gulf of Aqaba and the Gulf of Suez. Some details of the pull-apart structures in both gulfs are schematically shown in Figure 4 after *Daëron et al.* (2007) and *Garfunkel & Ben-Avraham* (1996). Further sources for drafting the tectonic scheme of Figure 4 are *Garfunkel et al.* (1981), *Barazangi* (1983), *Salamon et al.* (1996), *Papazachos & Papaioannou* (1999), *Khair et al.* (2000), *Meghraoui et al.* (2003), *Salamon et al.* (2003), *Akyuz et al.* (2006), *Nemer & Meghraoui* (2006), *Heidbach & Ben-Avraham* (2007), and *Hofstetter et al.* (2007). The western border of the Sinai block is, following *Mahmoud et al.* (2005) in its southern part, defined by the Gulf of Suez. In the N we introduce the modified PTF as part of the western border of the Sinai block. The northern border of the Sinai block is formed by the active Cyprian arc, which is linked tectonically with the SW end of the East Anatolian fault.

Deutsches GeoForschungsZentrum GFZ
Scientific Technical Report 09/09
DOI:10.2312/GFZ.b103-09098

4. Time-independent PSHA

4.1 Method

The probabilistic seismic hazard assessment used in this investigation is based on the method introduced by *Cornell* (1968, 1971) and implemented by *McGuire* (1976) as one of the early computer codes. This method requires to identify seismic source zones Src_i presuming each source having uniformly distributed seismicity (but not in depth). The probability of a ground shaking parameter A (e.g. peak ground acceleration PGA) to reach or exceed a certain value a at the site due to an earthquake occurring within Src_i can be computed as follows:

$$P_i[A \geq a] = \int_{V_i} \int_{m_{0i}}^{m_{max_i}} P_i[A \geq a \mid m, \vec{r}]\, f_{M_i}(m|\vec{r})\; f_{\vec{R}_i}(\vec{r})\, dm\, d\vec{r} \tag{1}$$

where $P_i[A \geq a \mid m, \vec{r}]$ is the conditional probability of occurrence or exceedence of a under the constraint of the earthquake having magnitude m and $\vec{r}$ being the distance vector between the event and the site, $f_{M_i}(m|\vec{r})$ is the conditional probability density of the magnitude distribution within Src_i and becomes $f_{M_i}(m)$ in the case of independent m and $\vec{r}$, and $f_{\vec{R}_i}(\vec{r})$ is the probability density of the distribution of the distance vectors. The distance vector is integrated over the whole volume V_i of the source Src_i, the magnitude is integrated from a minimum value m_{0_i} to the maximum value m_{max_i} which the source is able to produce.

A further parameter influencing A is the tectonic regime (tr) having the distribution $F_{TR_i}(tr)$ in Src_i. It can take the values N (**n**ormal faulting), S (**s**trike-slip faulting), and T (**t**hrust faulting), with the probability $P_i(tr)$, and can be introduced as a further constraint into the conditional probability of A:

$$\begin{aligned} P_i[A \geq a \mid m, \vec{r}] &= \int_{TR} P[A \geq a \mid m, \vec{r}, tr]\, dF_{TR_i}(tr) \\ &= \sum_{tr\, \epsilon\{N,S,T\}} P[A \geq a \mid m, \vec{r}, tr]\, P_i(tr) \end{aligned} \tag{2}$$

It is common to assume $P_i[A \geq a \mid m, \vec{r}]$ to be log-normally distributed and the ground motion prediction equations (GMPE) used in this study follow this assumption. Additionally, it is reasonable from practical point of view to truncate the uncertainties in ground motion. A commonly adopted practice is to truncate at two standard deviations.

The multiplication of $P_i[A \geq a]$ with the expected annual rate ν_{0_i} of earthquakes occurring in Src_i with a magnitude larger than or equal to m_0 results in the contribution $\nu_i(a)$ of source Src_i to the total expected annual rate $\nu_{tot}(a)$ of occurrence or ex-

Deutsches GeoForschungsZentrum GFZ
Scientific Technical Report 09/09
DOI:10.2312/GFZ.b103-09098

ceedence of the value a at the site:

$$\nu_{tot}(a) = \sum_i \nu_{0_i} \cdot P_i[A \geq a] \tag{3}$$

4.2 Seismicity data pre-processing for the PSHA

The seismicity data pre-processing consists of two steps: Firstly, the declustering, i.e. the removal of foreshocks and aftershocks, and secondly, the analysis of data completeness with time.

The declustering applied here follows the robust and rigorous method by *Grünthal* (1985), which was extended for its use for larger magnitudes, as described in *Burkhard & Grünthal* (2009) and in *Grünthal et al.* (2009b). Although originally developed for central European conditions, it proves not only be well applicable for this study but even for subduction zones (*Suckale & Grünthal* 2009). The effect of declustering is illustrated in Figure 6, which shows the number of events in half-magnitude classes in the SE Mediterranean area polygon before and after declustering. While the effect of declustering is indeed drastical up to $M_w = 4$, it is negligible for $M_w \geq 5.5$.

The analysis of magnitude-dependent data completeness with time follows the standard methodology we are successfully applying since more than 20 years. Since this approach has frequently been described in previous publications (e.g. *Burkhard & Grünthal* 2009 or *Suckale & Grünthal* 2009) we can be brief here. Basically, a magnitude bin is considered complete for the years in which a rough constant slope can be fitted to the cumulative number of earthquakes. The application of this approach to the entire DSFZ sensu lato results in the following magnitude dependent completeness periods:

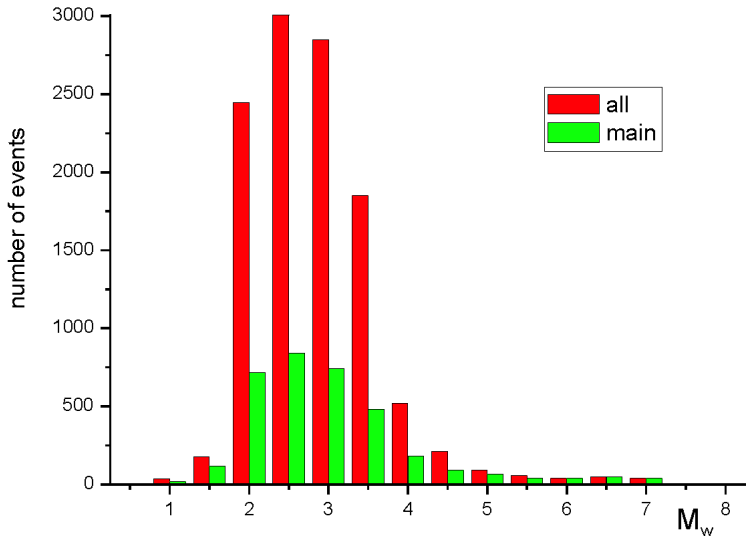

Figure 6. Effect of declustering within the used data set of this study. The numbers of events per magnitude class for the non-declustered data is shown by red columns and for the declustered data by green columns.

Deutsches GeoForschungsZentrum GFZ
Scientific Technical Report 09/09
DOI:10.2312/GFZ.b103-09098

$M_w = 3.5$ since 1985, $M_w = 4$ since 1960, $M_w = 4.5$ since 1960, $M_w = 5$ since 1920, $M_w = 5.5$ since 1890, $M_w = 6$ since 1720, $M_w = 6.5$ since 450 and $M_w = 7$ since 75 BC.

4.3 Ground motion prediction models

From a range of different GMPE we selected *Ambraseys et al.* (2005), *Akkar & Bommer* (2007), and *Pankow & Pechmann* (2004, 2006). The latter is an update of the approach by *Spudich et al.* (1999). *Ambraseys et al.* (2005) and *Akkar & Bommer* (2007) are based mostly on strong ground motion data recorded in the Middle East and in Europe. *Spudich et al.* (1999) selected a world-wide data set from areas with extensional tectonic regimes. Although *Ambraseys et al.* (2005) and *Akkar & Bommer* (2007) use basically the same data set, they represent two independent models to describe the ground motion attenuation with distance. All relations use moment magnitude. Also the applied distance metric, the Joyner-Boore distance, i.e. the closest horizontal distance to the vertical projection of the fault rupture to the Earth's surface, is common for all these GMPE.

Ambraseys et al. (2005) and *Akkar & Bommer* (2007) provide the possibility to distinguish between different faulting mechanisms. This is not the case with *Pankow & Pechmann* (2004, 2006). Hence we used the results from *Bommer et al.* (2003), who developed a method to derive coefficients for GMPE to characterize the different rupture mechanisms. These coefficients from *Bommer et al.* (2003) and *Bommer* (personal communication) derived for the GMPE from *Spudich et al.* (1999) could be applied in this study because *Pankow & Pechmann* (2004, 2006) use the same model and the same data as *Spudich et al.* (1999).

4.4 Seismic source zone model

The delineation of seismic source zones has been performed in two steps: (1) to define a large scale pattern which follows solely the large scale tectonic architecture, and (2) to subdivide the large scale pattern of seismic source zones into a set of small source zones, which reflect the spatial seismicity as well.

The four large scale zones (Fig. 7a) are

- the area along the DSFZ including the rim of seismic activity E and W of the DSFZ, and the Gulf of Aqaba as the southern extension of the DSFZ,
- the Gulf of Suez including the Red Sea triple junction S of Sinai,
- Cyprus and adjacent waters to the S and E,
- the southwesternmost part of the EAFZ including accompanying fault systems.

The model of seismic source zones is shown in Figures 7a and 7b, in Figure 7a together with the seismicity and in Figure 7b with the names of each source zone. The model gives to a certain extent credit to the model derived by *Abdallah et al.* (2006). Still, the two models show distinct differences, i.e. the model derived for this study can

Deutsches GeoForschungsZentrum GFZ
Scientific Technical Report 09/09
DOI:10.2312/GFZ.b103-09098

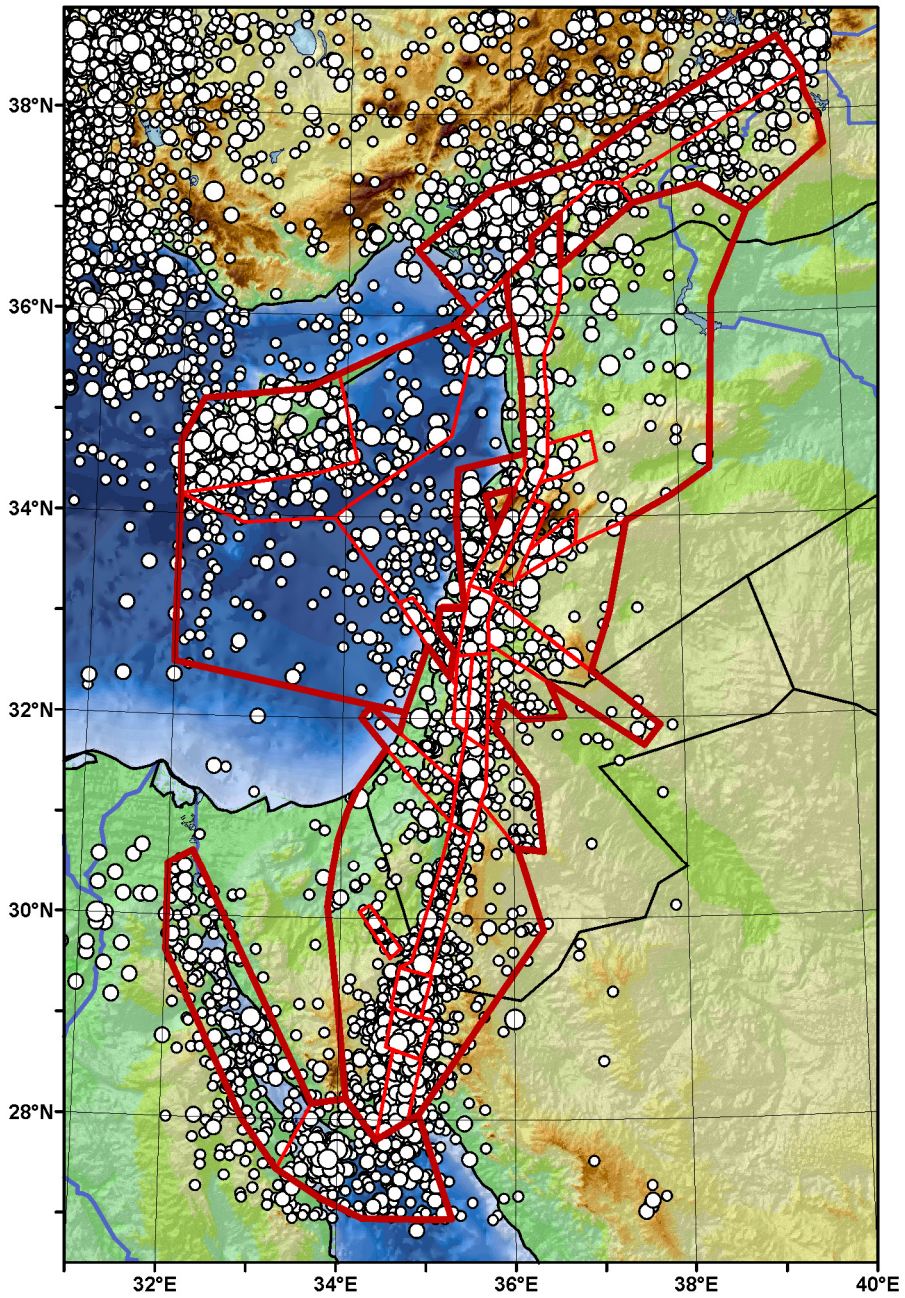

Figure 7a. The seismic source zone model in combination with the seismicity. The bold lines define the large scale zones.

be regarded as independent. The borders of the large scale zones are marked with bold lines. The DSFZ sensu stricto has been segmented into the following seismic source zones (from S to N)

- Wadi Arava/Araba,
- Dead Sea,
- Jordan Valley,
- Hula-Kinneret,
- Yammoûneh, Ghab and Kasaru (YGK).

Deutsches GeoForschungsZentrum GFZ
Scientific Technical Report 09/09
DOI:10.2312/GFZ.b103-09098

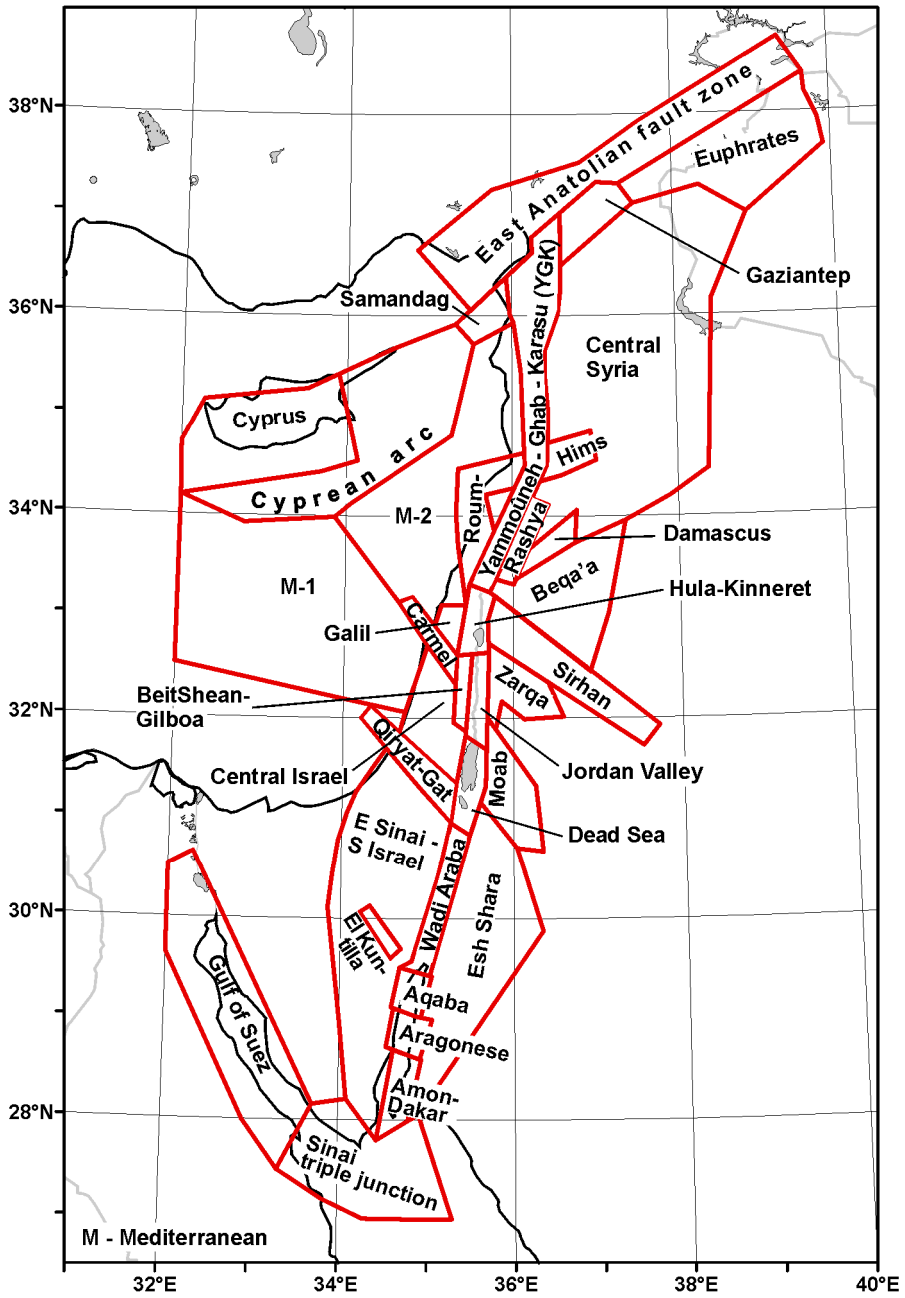

Figure 7b. The seismic source zone model with the notation of each source zone.

The seismicity E and W of the DSFZ could be associated in parts with known and with probable faults as they are indicated in Figure 2. Some of them are, e.g.: Carmel fault with its tentative off-shore extension, Roum fault, Palmyra fault and Mt. Lebanon thrust, Sirhan faults, Wadi Karak, El-Kuntilla epicentre alignment as well as a series of areal source zones with diffuse seismicity.

Along the Gulf of Aqaba the seismicity clusters spatially into three source zones. The seismicity at greater distances from the DSFZ, inasmuch it contributes to the seismic hazard of the target area of this study, does not require source zones which mirror the tectonic structures in great detail. This concerns roughly defined source zones for the Sinai triple junction and the Gulf of Suez, two zones for Cyprus and the active southern

Deutsches GeoForschungsZentrum GFZ
Scientific Technical Report 09/09
DOI:10.2312/GFZ.b103-09098

arc, and two source zones to encompass the seismicity in the off-shore areas between the Cyprus arc and the Levant. Three source zones have been introduced to model the SW part of the EAFZ, namely the EAFZ source zone itself, the Euphrates zone and further SW a zone which consists of two parts, Gaziantep and Samandag.

4.5 Seismicity parameters of the source zones

A seismic source zone is described, additional to its geometry, by three seismic activity parameters

- ν_0: the average yearly rate of events above or equal to a minimum magnitude m_0,
- β: the negative slope of the logarithm of the yearly rate in dependence of the magnitude,
- m_{max}: the maximum expected magnitude.

The non-cumulative frequency-magnitude relation $N(m)$ is in its classical form defined as the Gutenberg-Richter relation (*Gutenberg & Richter* 1954)

$$log\ N(m) = a - b\ m\ . \tag{4}$$

In exponential form the non-cumulative rate ν reads

$$\nu_{nc}(m) = exp(\alpha - \beta\ m) = 10^{a - b\ m}\ . \tag{5}$$

This relation holds within the magnitude range $m < m_{max}$, $exp(\alpha)$ is the value of ν_{nc} at $m = 0$. The cumulative yearly frequency $\nu(m)$ under consideration of m_0 and m_{max} is

$$\nu(m) = \nu_0 \frac{exp[\beta*(m_{max} - m)] - 1}{exp[\beta*(m_{max} - m_0)] - 1} \qquad m_0 \le m \le m_{max}\ . \tag{6}$$

The parameters ν_0 and β have been determined with the maximum-likelihood estimation after *Weichert* (1980) with the standard deviation σ of β.

Figures 8, 9 and 10 show the cumulative frequency-magnitude graphs for three large scale zones: The DSFZ, the SW part of the EAFZ, and the Cyprus zone. The b-values with their σ, and ν for given M_w are presented. We get remarkably straight-line fits over a broad range of magnitude classes. This can be seen as a quality sign of the used seismicity data file.

Deutsches GeoForschungsZentrum GFZ
Scientific Technical Report 09/09
DOI:10.2312/GFZ.b103-09098

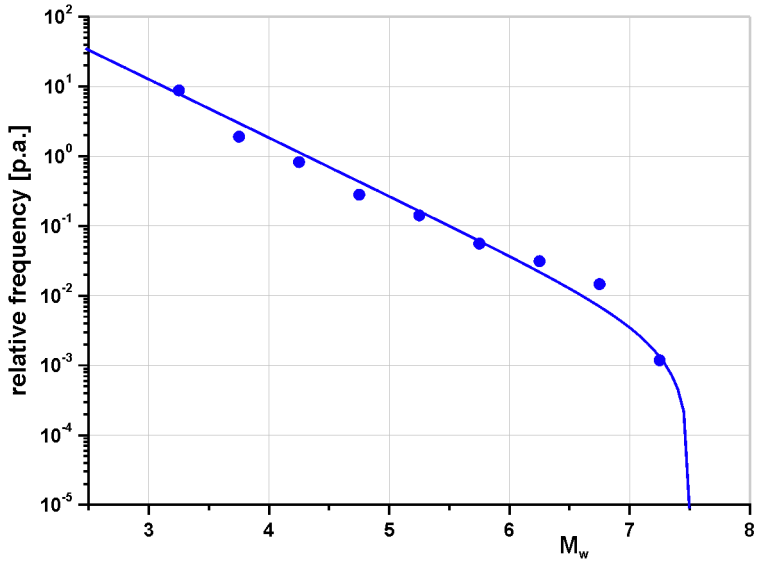

Figure 8. Frequency-magnitude relation for the entire Dead Sea fault zone (i.e. the large scale zone DSFZ), which is used as common-b area for small seismic source zones within the large zone. The b-value with its standard deviation is 0.838 ± 0.022. The frequency rate $\nu(M_w = 3.25)$ is 7.846.

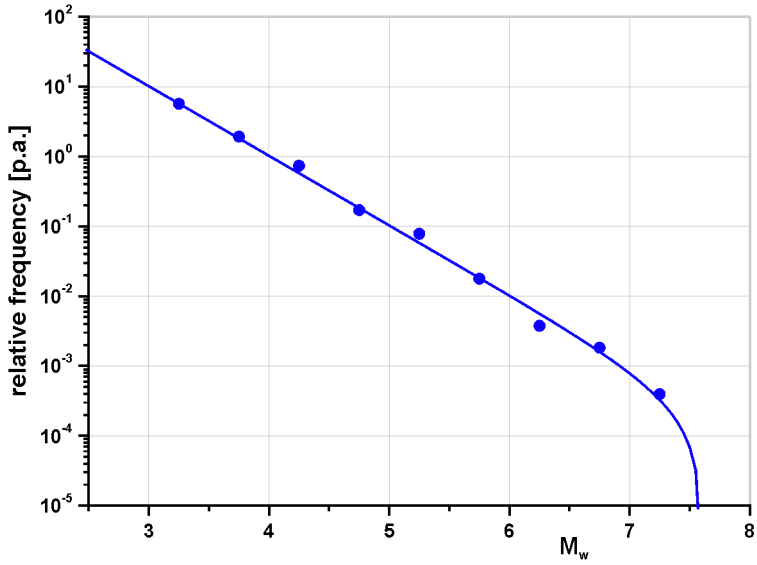

Figure 9. Frequency-magnitude relation for the southwestern part of the East Anatolian fault zone (i.e. the large scale zone EAFZ).
$b = 0.996 \pm 0.038$, $\nu(M_w = 3.25) = 5.721$.

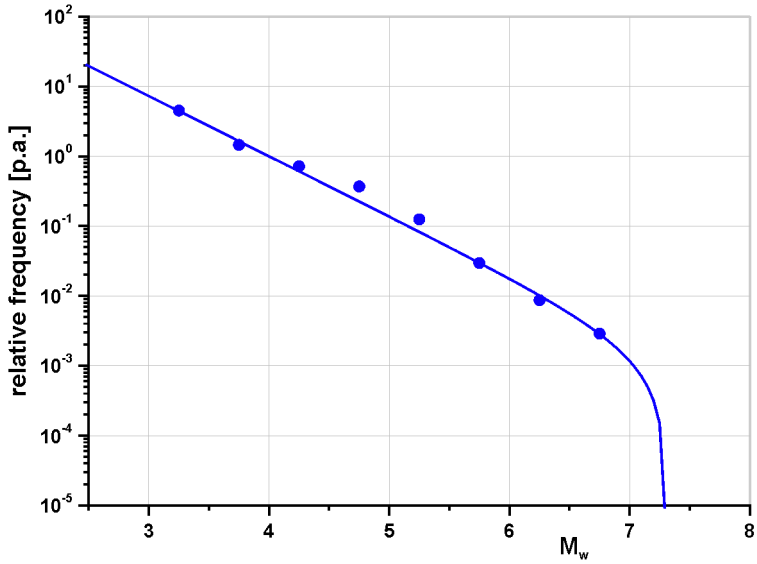

Figure 10. Frequency-magnitude relation for the large scale zone Cyprus.
$b = 0.861 \pm 0.031$, $\nu(M_w = 3.25) = 4.427$.

Deutsches GeoForschungsZentrum GFZ
Scientific Technical Report 09/09
DOI:10.2312/GFZ.b103-09098

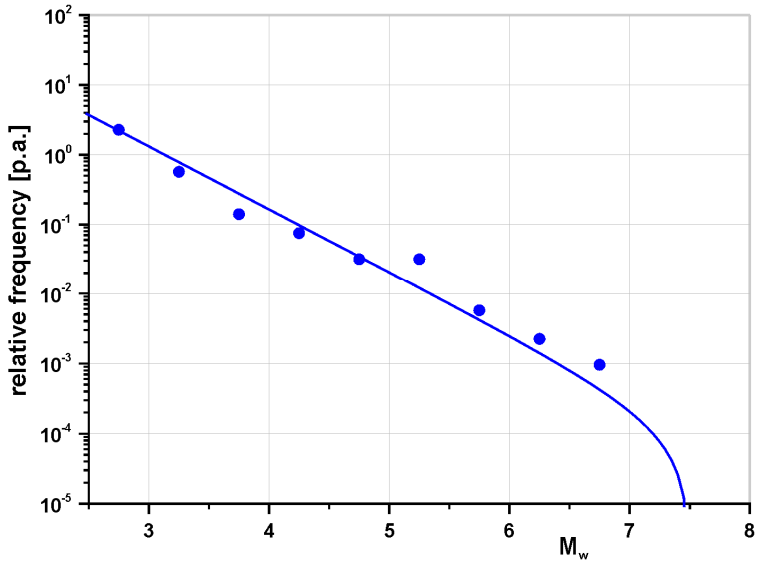

Figure 11. Frequency-magnitude relation for the small scale Dead Sea seismic source zone.
$b = 0.904 \pm 0.60$, $\nu(M_w = 2.75) = 2.214$.

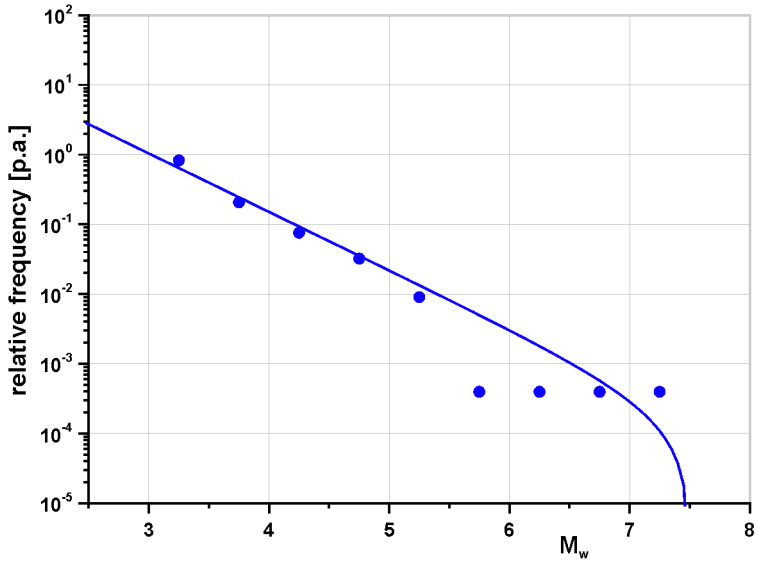

Figure 12. Frequency-magnitude relation for the small scale seismic source zone Aragonese in the central part of the Gulf of Aqaba.
$b = 0.838 \pm 0.022$, $\nu(M_w = 3.25) = 0.641$.

The determined occurrence rate of the $M_w = 7.3$ 1995 earthquake fits relatively well into the frequency-magnitude relation governed by the small magnitude earthquakes.

The b-values of the large zones are used for the small zones within the respective large zone area if the number of events in a small zone is below 50 within the complete magnitude ranges to be usable for the b-value determination. The only exception is Jordan Valley, which has less than 50 usable events, but a very good fit.

Figures 11 and 12 present two examples of frequency-magnitude relations for small scale source zones: (1) The Dead Sea source zone and (2) the central source zone within the Gulf of Aqaba (Aragonese), within which the $M_w = 7.3$ 1995 earthquake occurred. We can see that this event fits fairly well into the frequency-magnitude relation, governed by the frequencies of earthquakes of much smaller magnitudes, although three intermediate magnitude classes are empty.

The rationale with respect to estimate m_{max} for the seismic source zones along plate boundaries, like the DSFZ and the SW part of the EAFZ, was the assumption that during the almost two millennia of data the maximum magnitude has almost been experienced or even reached. The largest earthquakes along the DSFZ are three $M_w = 7.3$ events that occurred, in 847 AD in the northern Lebanon, in 1756 in 30 km NW of Damascus, and in 1995 in the

Deutsches GeoForschungsZentrum GFZ
Scientific Technical Report 09/09
DOI:10.2312/GFZ.b103-09098

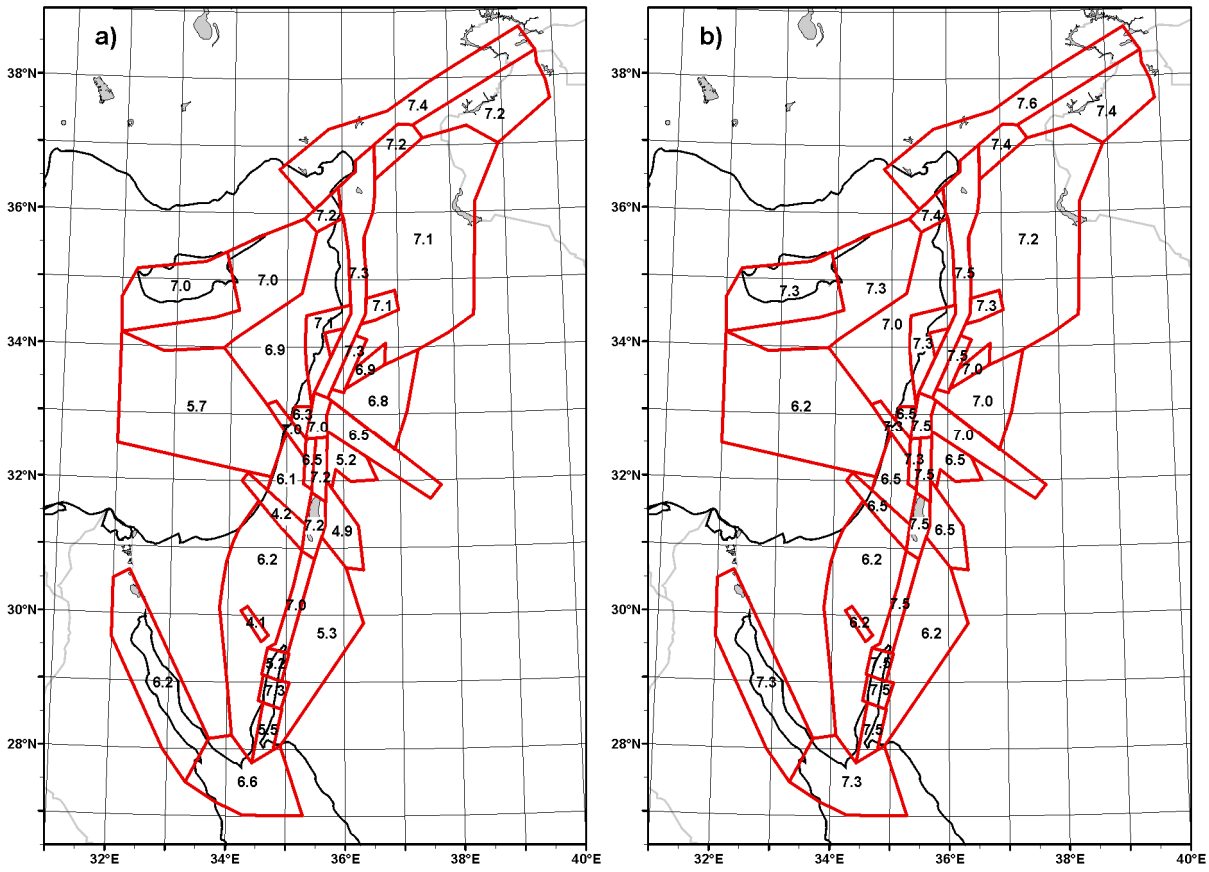

Figure 13. The maximum observed magnitudes (a) and the set maximum magnitudes in each seismic source zone. The set values are in the range of $M_w = 6.2 - 7.6$, i.e. the increments between the observed M_w and the set one are in the range 0-2.3.

Gulf of Aqaba. We assume that $M_w = 7.3$ is near to m_{max} and introduce a small increment of 0.2 to yield $m_{max} = 7.5$ for all source zones along the DSFZ. The maximum observed M_w is in no seismic source zone along the DSFZ N of Aqaba below 7.0. Along the SW part of the EAFZ, which is part of the study area, $m_{max,obs} = 7.4$. With the same increment as mentioned above, we get $m_{max} = 7.6$ here. Within the seismic source zones covering Cyprus and the off-shore part S thereof with $m_{max,obs} = 7.0$ we introduce an increment of 0.3 to yield $m_{max} = 7.3$. In the remaining seismic source zones m_{max} is in the range of 6.2 to 7.3 with increments between 0 and 2.3. The increment was assumed to be small (or even zero) in areas where an isolated large magnitude entry exists and where the seismicity otherwise is inconspicuous. On the other hand, in the off-shore source zones in the Gulf of Aqaba neighbouring the one with the $M_w = 7.3$ 1995 event and where $m_{max,obs}$ is smaller than $M_w = 6$, the increment is large in order to have $m_{max} = 7.5$ consistent along the entire DSFZ. All observed and estimated maximum magnitudes are given in Figure 13.

The focal depth is another parameter characterizing a seismic source zone and is needed in PSHA. Five values are selected for each of the large scale zones from the largest events with sufficiently well determined depth. These were then assigned to each small scale source zone within the respective large scale zone. These obtained depth values are given in Table 2. They range between 5 and 45 km.

Deutsches GeoForschungsZentrum GFZ
Scientific Technical Report 09/09
DOI:10.2312/GFZ.b103-09098

Table 2. Focal depths (km) representative for the four large scale zones within groups of source zones

DSFZX	5	9	11	15	30
EAFZ	5	7	10	20	45
CYPX	10	10	24	26	30
GOSZ	5	6	7	10	20

DSFZX – Dead Se fault zone without off-shore areas included in CYPX, EAFZ – East Anatolian fault zone, CYPX – Cyprus and off-shore areas S and E of the island, GOSZ – Gulf of Suez and the Sinai triple junction

4.6 Resulting time-independent PSHA and comparison with previous studies

The seismic hazard has been calculated for the Levant area from 29°-37°N and up to 37.4°E by using the software package FRISK88M (*Risk Engineering Ltd.* 1997) for points of a grid with a 0.1 × 0.1 degree spacing. As ground motion parameters we chose peak ground acceleration (PGA) and spectral ground accelerations (SGA). The integration of aleatoric uncertainties in the GMPE was performed up to two standard deviations σ. All calculations are given for rock conditions. In order to compare our results with previous PSHA studies for the DSFZ, given as mean values of ground motion parameters, we present our results as mean values as well. The restriction to mean values does not require to consider the full range of uncertainties in the input parameters and models. This will be the subject of a coming up study. Figure 14 shows typical hazard curves in terms of PGA, here for the cities of Nablus and Jerusalem.

Figures 15 and 16 present seismic hazard maps for the PSHA target area of this study for PGA and SGA at 5 Hz for the hazard level of 10% exceedence probability within 50 years. Depicted are the mean values for rock conditions. The seismic hazard along the

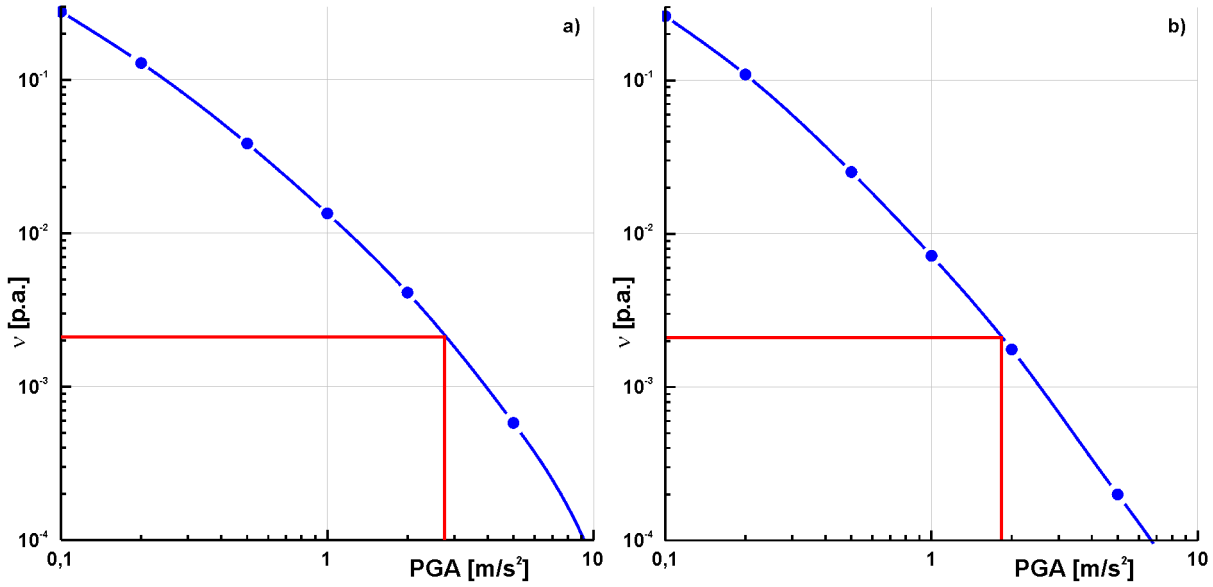

Figure 14. Seismic hazard curves in terms of mean ground acceleration (PGA) for the cities of Nablus **(a)** and Jerusalem **(b)** for the soil type rock. Indicated is the PGA value for the 10% exceedence probability within 50 years, which corresponds to a mean return period $T = 475$ years or an annual occurrence probability $\nu = 2.10 \cdot 10^{-3}$.

Deutsches GeoForschungsZentrum GFZ
Scientific Technical Report 09/09
DOI:10.2312/GFZ.b103-09098

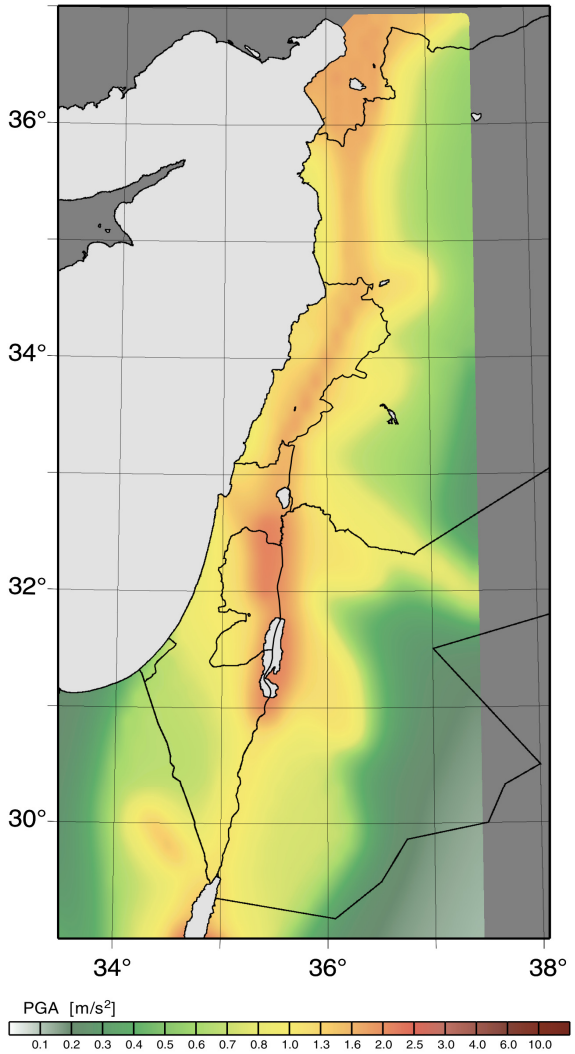

Figure 15. Seismic hazard map for the Levant in terms of peak ground accelerations PGA for 10% exceedence probability within 50 years, mean values and for the soil type rock.

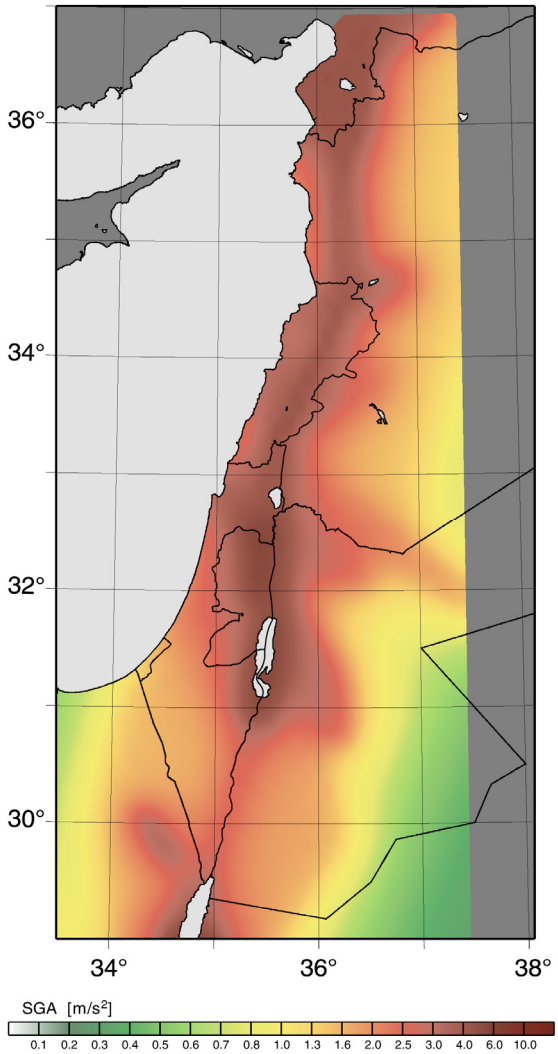

Figure 16. Seismic hazard map for the Levant in terms of spectral ground acceleration SGA for 10% exceedence probability within 50 years for 5 Hz, mean values and for the soil type rock.

DSFZ turns out to be lowest along the Arava fault, and highest in the Jordan valley S of Lake Kinneret, in the Dead Sea area, and at the northernmost part of the DSFZ along the Karasu fault.

A comparison of the mean PGA values according to this study can be made with nine previous studies. These are (in reverse chronological order): *Al-Tarazi & Sandvol* (2007), *Jiménez et al.* (2006), *Abdallah et al.* (2006), *Elnashai & El-Khoury* (2004), *Harajli et al.* (2002), *Al-Tarazi* (1999), Mayer-Rosa & Selami (in *Grünthal et al.* 1999), *Husein Malkawi et al.* (1995), and *Arieh & Rabinowitz* (1989). Table 3 shows the interesting fact that the seismic hazard according to this study yields the lowest PGA at the two selected points where all studies overlap.

Deutsches GeoForschungsZentrum GFZ
Scientific Technical Report 09/09
DOI:10.2312/GFZ.b103-09098

Table 3. PGA values according to this study compared with previously published PSHA values at two selected sites where the compared hazard maps overlap.

	PGA (m/s^2) at	
	33°N, 35.5°E	**33°N, 36°E**
This study	1.60	0.96
Al-Tarazi & Sandvol (2007)	1.9	1.5
Jiménez et al. (2006)	2.1	1.3
Abdallah et al. (2006)*	1.8/2.2	1.1/1.5
Elnashai & El-Khoury (2004)	1.91	1.27
Harajli et al. (2002)	2.7	1.35
Al-Tarazi (1999)	3.8	2.6
Mayer-Rosa & Selami (1999)**	2.67	1.97
Husein Malkawi et al. (1995)	5.0	4.6
Arieh & Rabinowitz (1989)	2.3	1.1

* The two PGA values are due to the usage of different GMPE; the lower values are according to *Ambraseys et al.* (1996) and the larger ones according to *Boore et al.* (1997).
** Published as contribution for the Eastern Mediterranean region for GSHAP in *Grünthal et al.* (1999).

There are mainly three elements in PSHA which are most probably the reason for the considerable scatter from study to study. The first one is due to the selected GMPE or a set of these as is the case for this study. Significant progress has recently been made in this respect. Nevertheless, weaknesses in rather modern GMPE have already been observed and will be the subject of future innovations. These have to be considered in an envisaged update of this study.

The second element is due to considerable uncertainties in the cataloguing of earthquakes and in deriving harmonized and reliable magnitudes for the used seismicity data base. Previous studies had to be based on less credible magnitude estimates and could contain fake events.

The third element, observed in many previous PSHA studies, is due to methodological uncertainties in the entire data handling for deriving the input for a PSHA as well as methodological weaknesses in performing the entire multi-integration in the frame of the PSHA itself.

5. Developed time-dependent approach to PSHA

5.1 Method

5.1.1 Earthquake occurrence rate

The earthquake occurrence rate ν demonstrates the number of events (here earthquakes above a certain magnitude threshold) in a time unit at a generic time. The mathematical interpretation of the occurrence rate is:

$$\nu(t) = \lim_{\Delta t \to 0} P\left[t \le T \le t \pm \Delta t \mid T \ge t\right] = \frac{f(t)}{S(t)} \tag{7}$$

Deutsches GeoForschungsZentrum GFZ
Scientific Technical Report 09/09
DOI:10.2312/GFZ.b103-09098

where $f(t)$ is the probability density function (*pdf*) corresponding to the distribution of the inter-event times (i.e. the time between two consecutive events of interest), and $S(t)$ is the survivor (or reliability) function defined as:

$$S(t) = 1 - F(t) \quad with \quad F(t) = \int_0^t f(x)\,dx \tag{8}$$

where $F(t)$ is known as the distribution or cumulative distribution function (*cdf*). In general, there are two types of occurrence rates, time-dependent and time-independent. Time-dependent occurrence rates change with time, e.g. the occurrence rates corresponding to Weibull or Gamma distributions. Time-independent occurrence rates extracted from exponential distributions (Poisson processes) do not change with time.

5.1.2 Time-dependent modelling of earthquake occurrence rates

In order to model the earthquake occurrence rate, a statistical approach has been adapted and applied to find the distribution of the earthquake inter-event times (recurrences) of large earthquakes. The approach has been developed based on the assumption that earthquake inter-event times are independently identically distributed. This assumption leads to a renewal process assumption for the inter-event times (*Taylor & Karlin* 1998).

In order to model the inter-event times of the large earthquakes, five candidate models have been selected and tested. The models include the time-independent exponential as well as the time-dependent Weibull, Gamma, Lognormal, and inverse Gaussian (Brownian Passage Time BPT) distributions. Here, the time dependence describes whether the hazard function, corresponding to a specific distribution, is a function of time (time-dependent) or not (time-independent). A bootstrap multimodality test (*Efron & Tibshirani* 1993) has been applied to check whether the inter-event times are unimodally or multimodally distributed. The five distributions have been directly used for the case of unimodal distributions, while the four time-dependent distributions have been considered as basic models involved in the structure of multimodal distributions, where multimodality is applicable.

The maximum likelihood estimation method (MLE) has been modified (see *Hakimhashemi* 2009) to estimate the parameters of the different distributions. Two important terms, with respect to the subject of this study, have been added to the classic method of MLE. The first one is the censored time which is important in time-to-failure modelling, since it includes the most recent information related to the current situation of a given time-to-failure process. The second term is the weighting information which leads to the use of a weighted MLE. The reason to use the weighted information is that the intrinsic uncertainty of historical earthquake data is neither recognizable, nor calculable. Therefore, the estimation process requires larger weights for earthquakes occur-

Deutsches GeoForschungsZentrum GFZ
Scientific Technical Report 09/09
DOI:10.2312/GFZ.b103-09098

ring in the recent time.

The best distribution has been selected according to two criteria, a Bayesian Information Criterion (BIC) and a Kolmogorov-Smirnov test (KS-test) p-value. Finally, the confidence intervals have been calculated by a bootstrap confidence interval method for each parameter corresponding to the selected models. More details about the method can be found in *Hakimhashemi* (2009).

5.1.3 Application of the time-dependent earthquake occurrence rate to probabilistic seismic hazard assessment

Time-dependent earthquake occurrence rates change with time. Suppose that t is a generic time after an earthquake occurrence, then $\nu_{0_i}(t)$ is a non-constant function of t. Considering a time-dependent hazard function ν_{0_i} in PSHA equations in section 4.1 changes to $\nu_{0_i}(t)$ which is time-dependent. Then the PSHA equation (3) changes to

$$\nu_{\mathrm{tot}}(t, a) = \sum_i \nu_{0_i}(t)\ P_i(A \geq a) \tag{9}$$

The PSHA is generally estimated during some fixed time span in the future. In the case of time-independent PSHA, the seismic hazard in a given time unit (e.g. annual seismic hazard) remains constant with time. In contrast, in time-dependent PSHA, the hazard function $\nu_{\mathrm{tot}}(t, a)$ changes with time. In order to calculate time-dependent hazard ν_{tot} during a time span $[t, t + \Delta t]$, the $\nu_{0_i}(t)$ in equation (9) can be replaced by:

$$\frac{1}{\Delta \mathrm{t}} \int_{\mathrm{t}}^{\mathrm{t}+\Delta \mathrm{t}} \nu_{0_i}(\tau)\, \mathrm{d}\tau\ . \tag{10}$$

According to equation (10), considering larger time spans results in loosing details of seismic hazard variations with time. Therefore, the time span has to be carefully considered and as short as possible, especially in cases in which the seismic hazard varies vividly with time.

In this study the time-dependent portion of the seismic hazard has been prepared considering earthquakes with $M_w \geq 6$. For the rest; i.e. earthquakes with $M_w < 6$, the seismic hazard has been calculated using the classical time-independent approach (Poisson process). The total seismic hazard has been obtained by aggregating the time-dependent and the time–independent portions.

Deutsches GeoForschungsZentrum GFZ
Scientific Technical Report 09/09
DOI:10.2312/GFZ.b103-09098

5.2 Application of the method to the DSFZ

The method has been applied to the central and northern parts of the DSFZ, but not to the southern part because of the lack of data (see *Hakimhashemi* 2009). The central part of the DSFZ covers the three seismic source zones Dead Sea, Jordan Valley, and Hula-Kinneret. The northern part of the DSFZ is represented by the two seismic source zones YGK (Yammoûneh, Ghab, Karasu) and Rashya for $M_w < 6$. For $M_w \geq 6$ both are handled for the PSHA as one source zone.

The results for the central part of the DSFZ show that the time-dependent model is not significantly better than the time-independent model. Since the time-independent model is simpler to interpret, the occurrence rate of large earthquakes in this area has been considered as the classical time-independent occurrence rate.

According to the dataset of the northern part of the DSFZ, the last $M_w \geq 6$ earthquake in this area occurred in 1872. Therefore, the time since the last earthquake (i.e. the censored time) is 137 years. The average observed earthquake inter-event time in this area is about 51 years, i.e. much smaller than 137 years. Another fact is that more than 96% of inter-event times in this area are shorter than the censored time. Furthermore, the earthquake inter-event times in the northern part of the DSFZ reveal a clustering property. The inter-event time dataset can be divided into two different parts, one with inter-event times shorter than 37 years, another with inter-event times larger than 65 years (Fig. 17). This clustering property is also an indication of multimodality of the earthquake inter-event times in this area.

The first step of the estimation process is to check if the distribution of the earthquake inter-event times in this area is multimodal. The results of the test indicate that there is no significant difference between unimodality and bimodality. Therefore, the

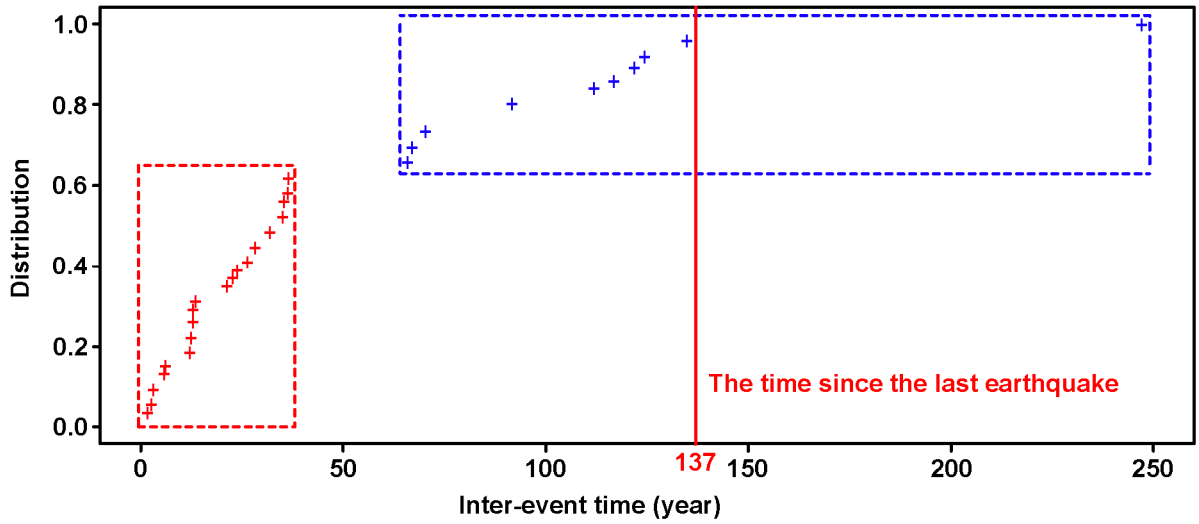

Figure 17. A schematic clustering behaviour of the inter-event times for earthquakes with $M_w \geq 6$ in the northern part of the DSFZ (seismic source zones YGK and Rashya). The crosses present the empirical distribution function, red crosses show the first cluster, and blue crosses demonstrate the second cluster. The red vertical line shows the censored time and how it compares with inter-event times.

Deutsches GeoForschungsZentrum GFZ
Scientific Technical Report 09/09
DOI:10.2312/GFZ.b103-09098

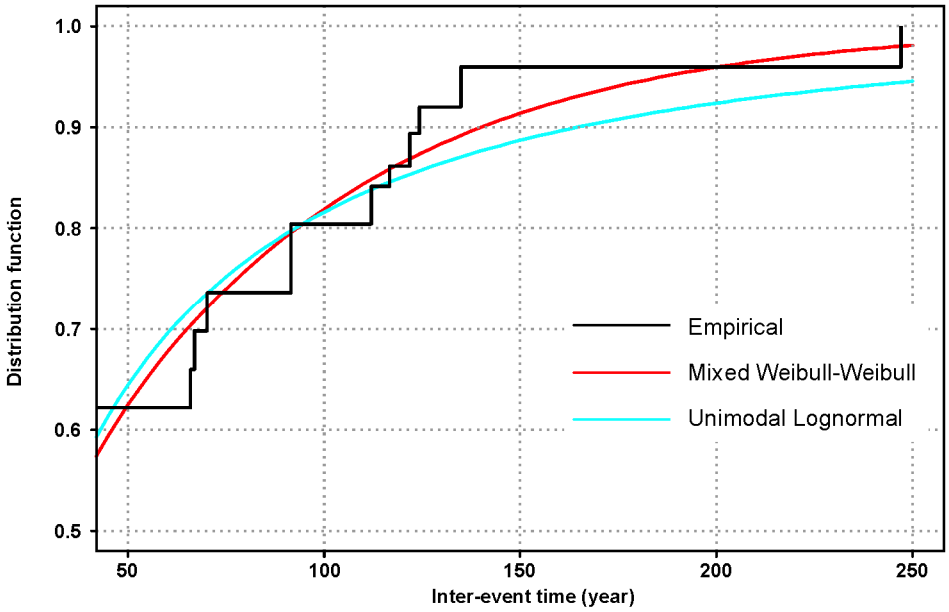

Figure 18. Comparison between the mixed Weibull-Weibull, the unimodal Lognormal, and the empirical distribution functions of earthquake inter-event times for the northern part of the DSFZ (seismic source zones YGK and Rashya). Results for longer inter-event times and magnitudes larger than 6 are shown.

distribution of the earthquake inter-event times is estimated under both assumptions; i.e. unimodality and bimodality. Based on the BIC and KS-test p-value (section 5.1.2), the best unimodal distribution for the northern part of the DSFZ is the Lognormal distribution and the best bimodal distribution is the mixed Weibull-Weibull distribution. These models have been compared, focusing only on the longer inter-event times, i.e. inter-event times larger than 60 years considering the sum of squared errors (SSE = Σ [estimate − observed]^2). The mixed Weibull-Weibull distribution can fit this part of inter-event times better than the unimodal Lognormal distribution (Fig. 18). This result plays an important role in the process of selecting the best model, as the time since the last $M_w \geq 6$ earthquake (i.e. censored time) is much larger than the average earthquake inter-event time. Another advantage of the Weibull-Weibull distribution is its bi-cluster shape which can describe the long-term clustering behaviour in this area better than the unimodal Lognormal distribution.

5.3 Occurrence rates of candidate models in the northern part of the DSFZ

Figure 19 shows how the hazard function of the mixed Weibull-Weibull distribution increases immediately after the 1872 earthquake occurrence to a maximum value (about 0.024), then decreases to a minimum value (about 0.015 after about 80 years), and after that increases very slowly with time. In contrast, the hazard function of the unimodal Lognormal distribution also increases immediately after the earthquake occurrence to a maximum value (about 0.026), then decays with the time. Among these two completely different trends, an increasing (the mixed Weibull-Weibull) and a de-

Deutsches GeoForschungsZentrum GFZ
Scientific Technical Report 09/09
DOI:10.2312/GFZ.b103-09098

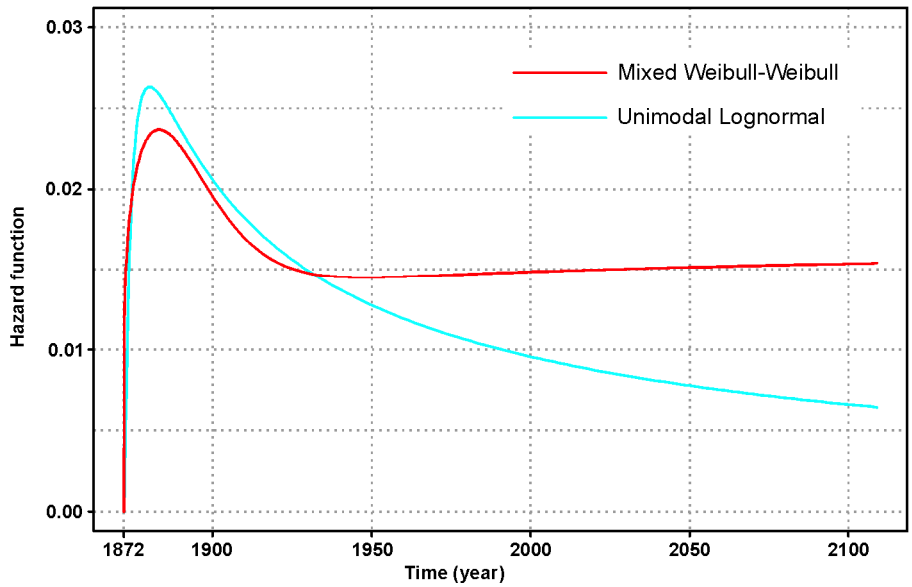

Figure 19. The trends of hazard functions of the mixed Weibull-Weibull and the unimodal Lognormal distributions after the last earthquake in 1872. The mixed Weibull-Weibull model has an increasing hazard function in the long-term.

creasing (the unimodal Lognormal) hazard function for the long-term, an increasing hazard function for the long-term is selected due to the long-term clustering behaviour. The mixed Weibull-Weibull distribution is selected to model the inter-event times of $M_w \geq 6$ earthquakes in the northern part of the DSFZ.

5.4 Hazard maps produced for the entire DSFZ using candidate models

Following equations (9) and (10), the time-dependent PSHA has been calculated for the northern part of the DSFZ. Figures 20–24 demonstrate the hazard maps produced for the northern part of the DSFZ using the mixed Weibull-Weibull, the Lognormal, and the exponential (classical time-independent under Poisson process) distributions. The maps are prepared for different years after the last $M_w \geq 6$ earthquake in the northern part of the DSFZ, i.e. 1873, 1875, 1883, 2009, and 2100. The hazard maps have been prepared considering earthquakes with magnitude $M_w \geq 6$ in the considered source zone (see Fig. 20).

Deutsches GeoForschungsZentrum GFZ
Scientific Technical Report 09/09
DOI:10.2312/GFZ.b103-09098

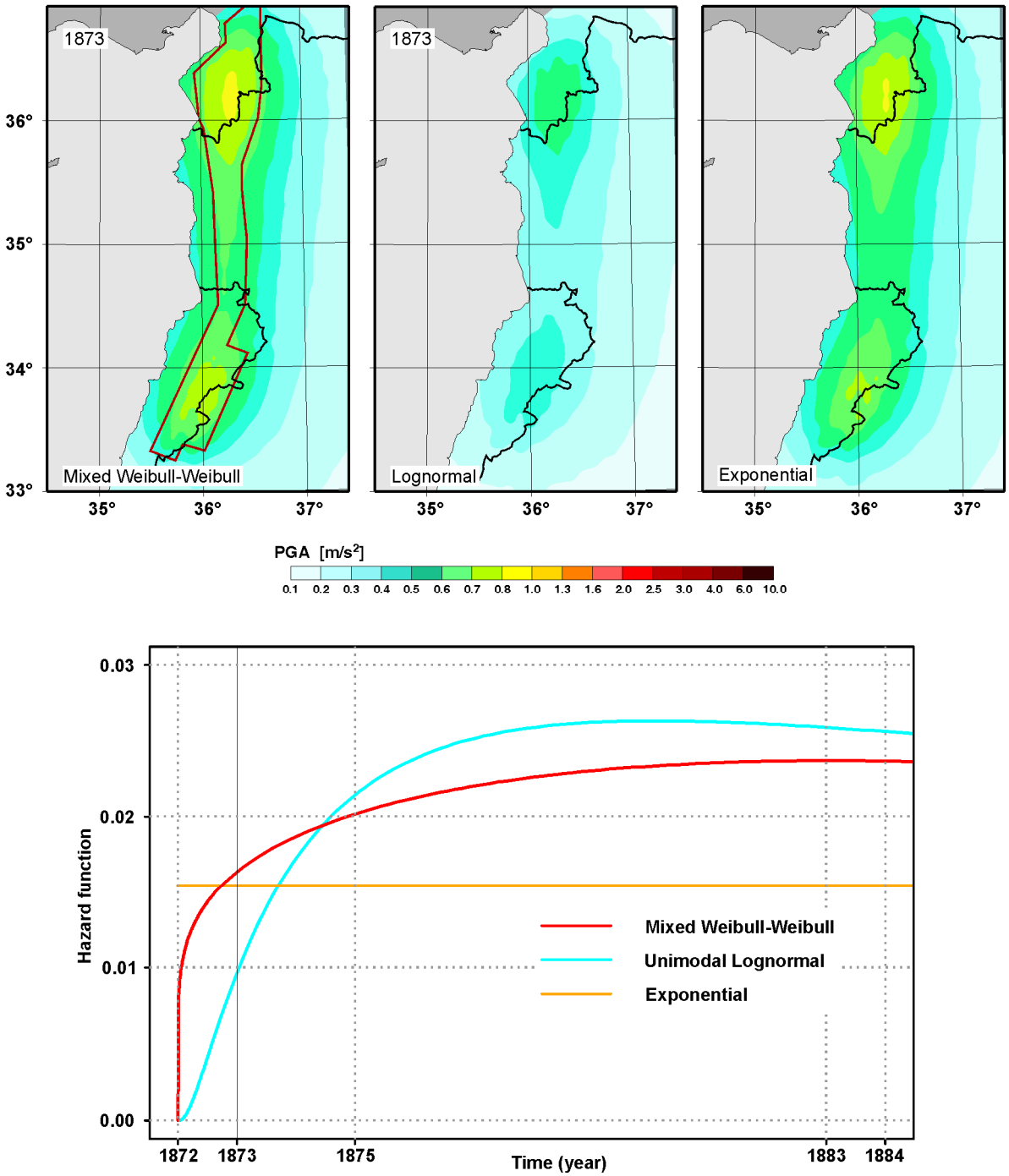

Figure 20. Top: Hazard maps for the northern part of the DSFZ (seismic source zones YGK and Rashya) in the year 1873 for 10% exceedence probability in 50 years considering occurrence rates of large events obtained by the mixed Weibull-Weibull, the unimodal Lognormal, and the exponential distributions (classical time-independent model under the Poisson process). The red polygon shows the boundary of the source zone. Bottom: Statistical hazard functions (occurrence rates) for the mixed Weibull-Weibull, the unimodal Lognormal, and the exponential distributions within 1872-1884.

Deutsches GeoForschungsZentrum GFZ
Scientific Technical Report 09/09
DOI:10.2312/GFZ.b103-09098

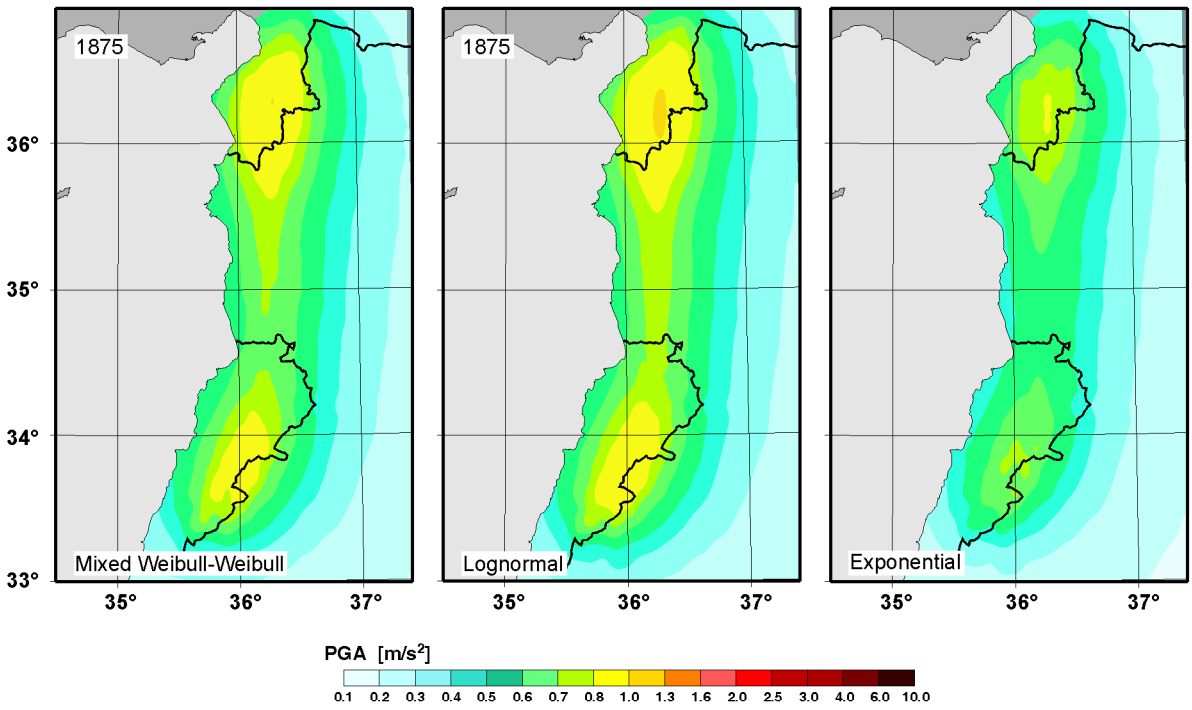

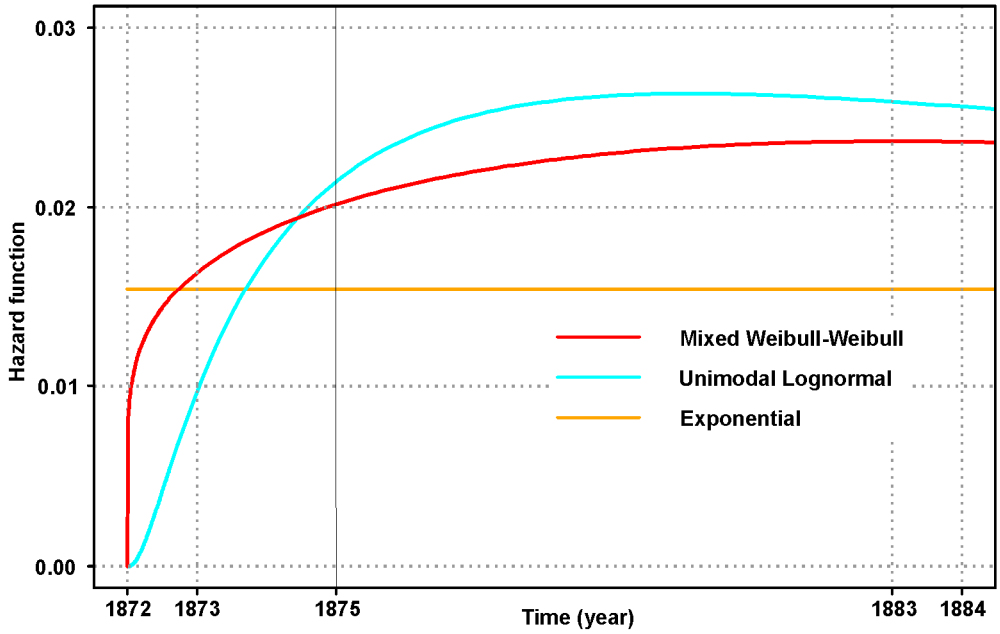

Figure 21. Same as Figure 20 for the year 1875.

Deutsches GeoForschungsZentrum GFZ
Scientific Technical Report 09/09
DOI:10.2312/GFZ.b103-09098

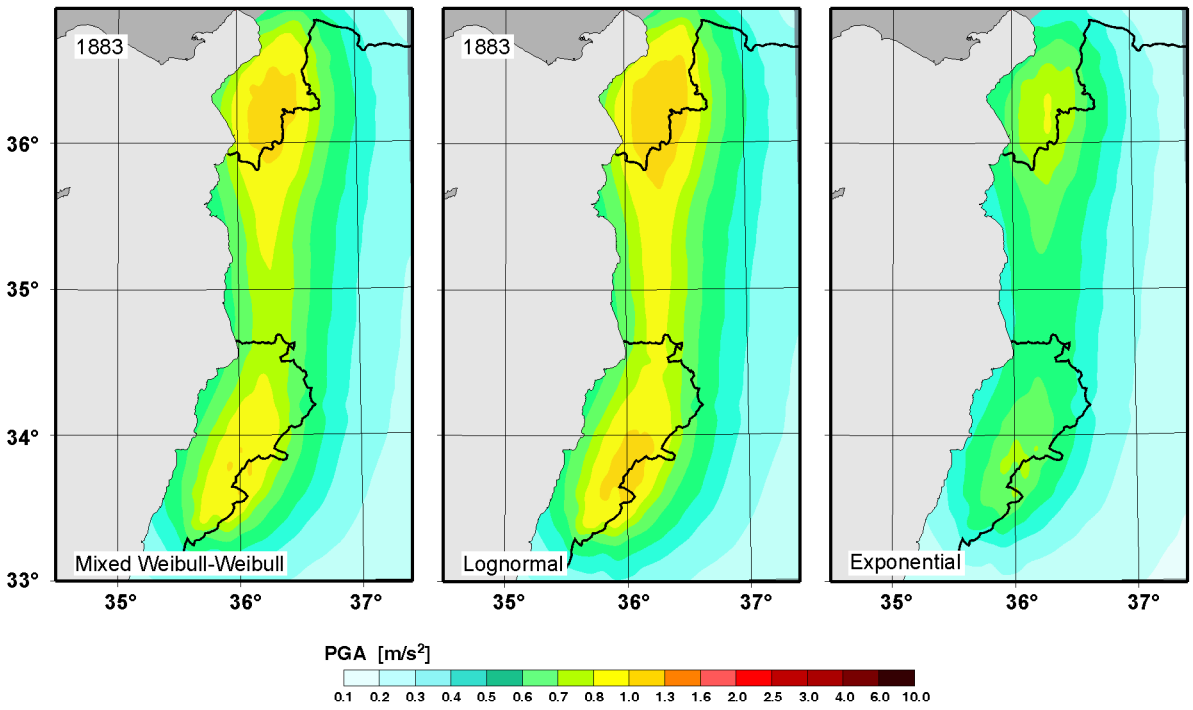

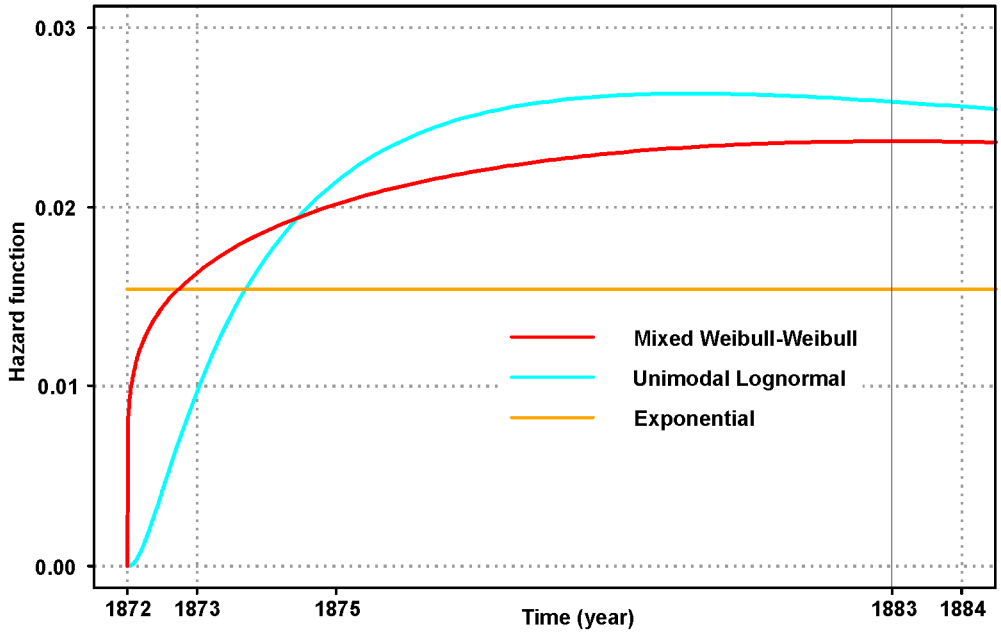

Figure 22. Same as Figure 20 for the year 1883.

Deutsches GeoForschungsZentrum GFZ
Scientific Technical Report 09/09
DOI:10.2312/GFZ.b103-09098

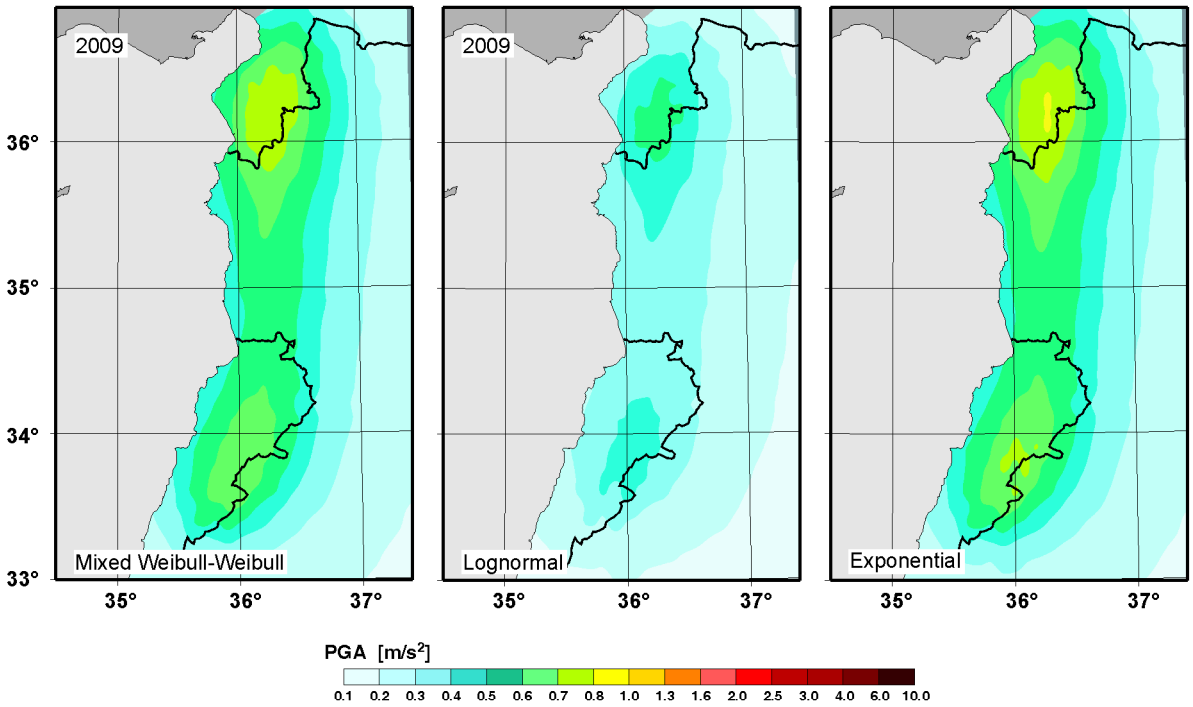

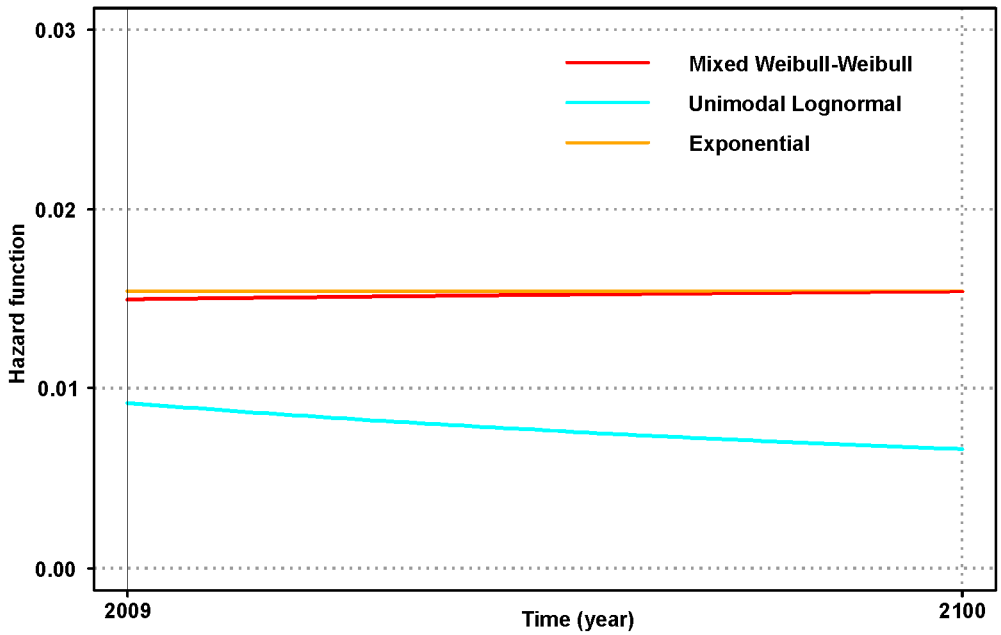

Figure 23. Same as Figure 20 for the year 2009 and hazard functions within 2009-2100.

Deutsches GeoForschungsZentrum GFZ
Scientific Technical Report 09/09
DOI:10.2312/GFZ.b103-09098

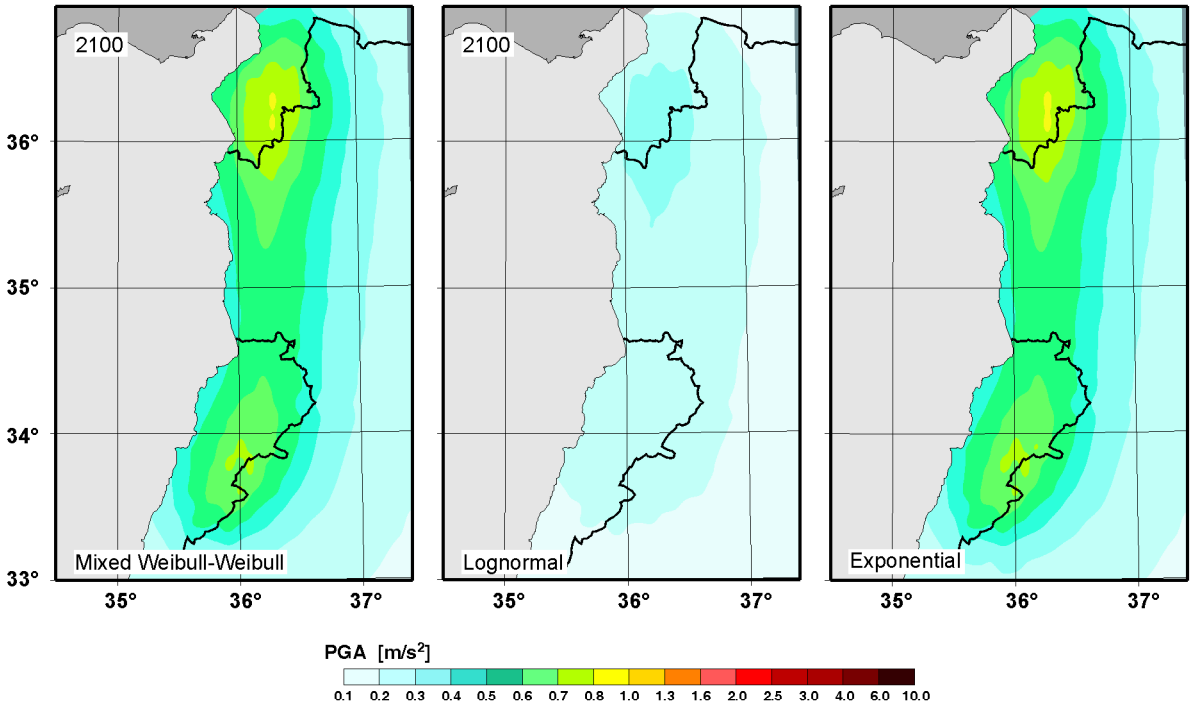

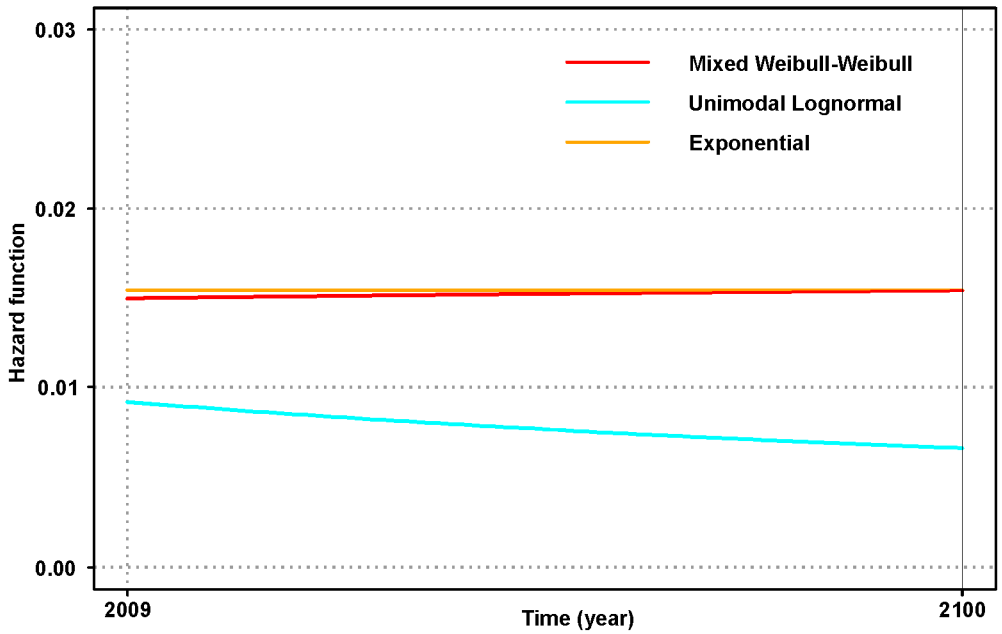

Figure 24. Same as Figure 23 for the year 2100.

Deutsches GeoForschungsZentrum GFZ
Scientific Technical Report 09/09
DOI:10.2312/GFZ.b103-09098

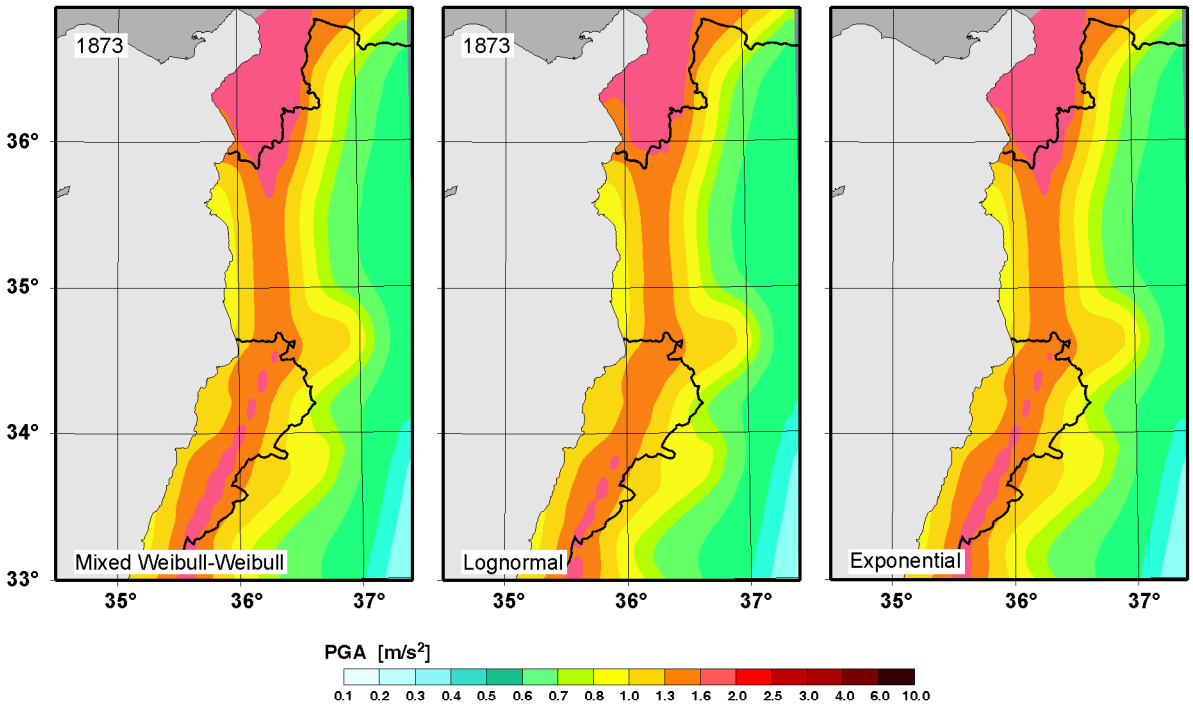

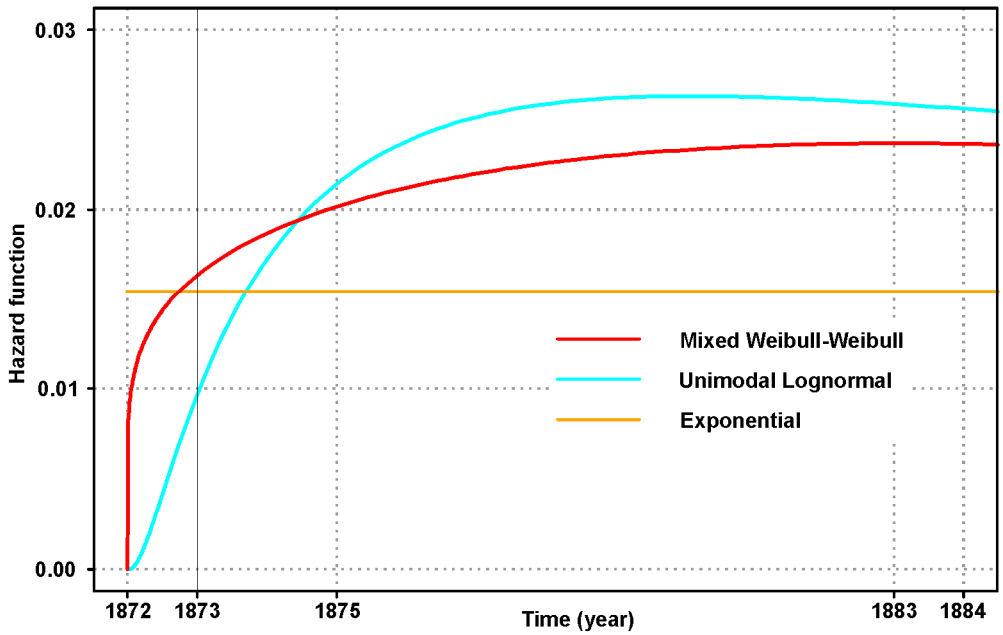

Figure 25. Same as Figure 20 but using the whole data set.

Deutsches GeoForschungsZentrum GFZ
Scientific Technical Report 09/09
DOI:10.2312/GFZ.b103-09098

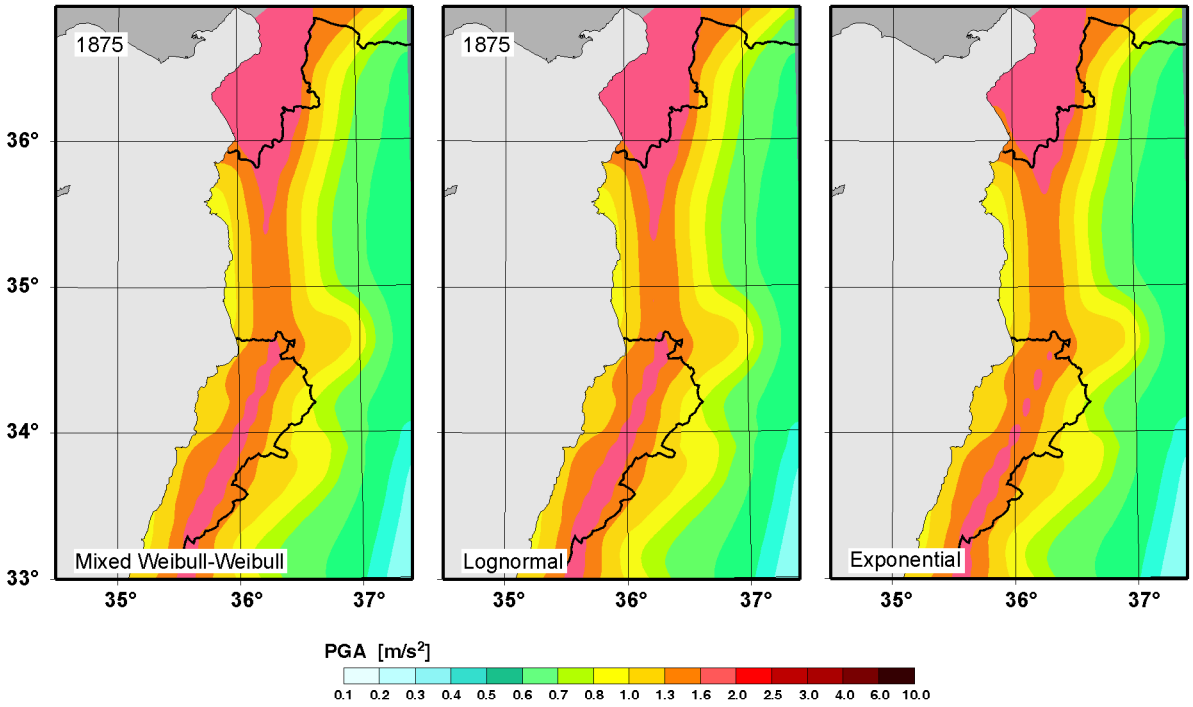

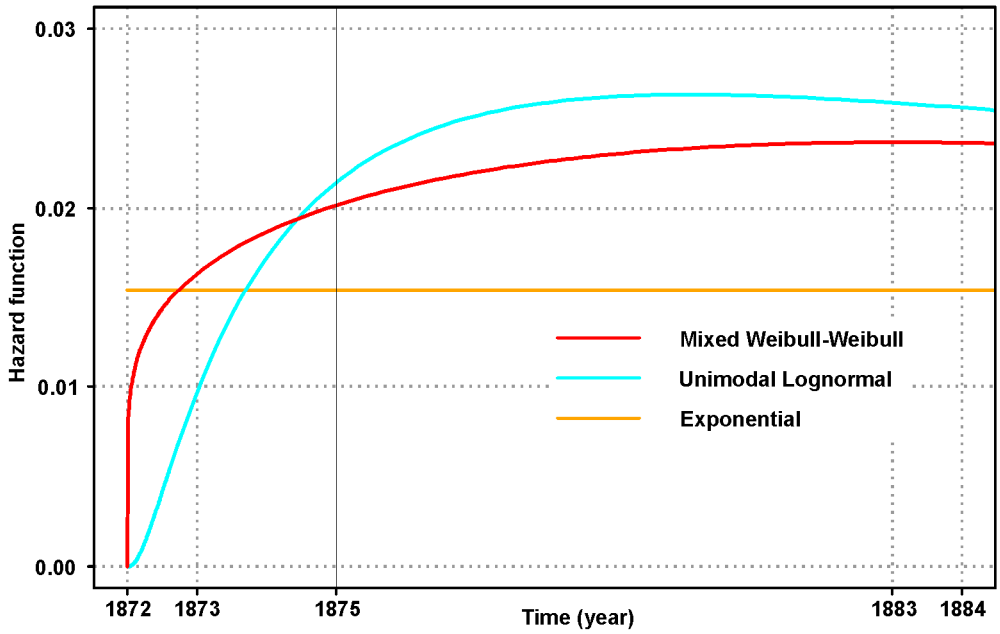

Figure 26. Same as Figure 21 but using the whole data set.

Deutsches GeoForschungsZentrum GFZ
Scientific Technical Report 09/09
DOI:10.2312/GFZ.b103-09098

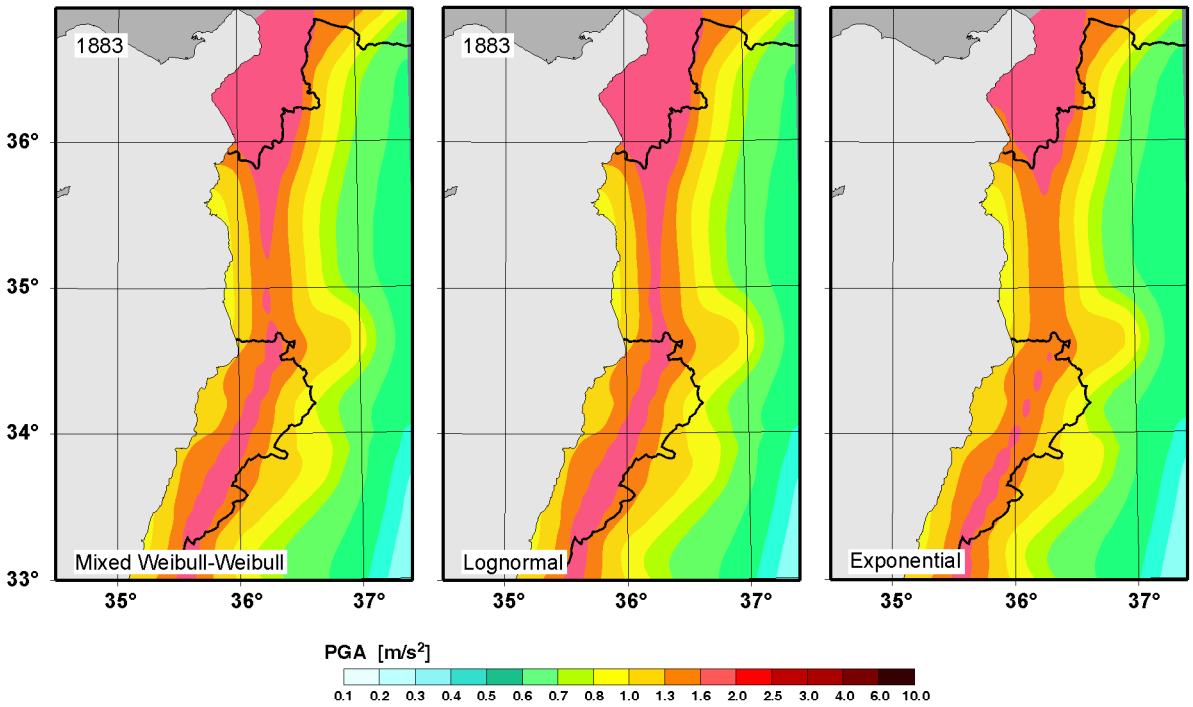

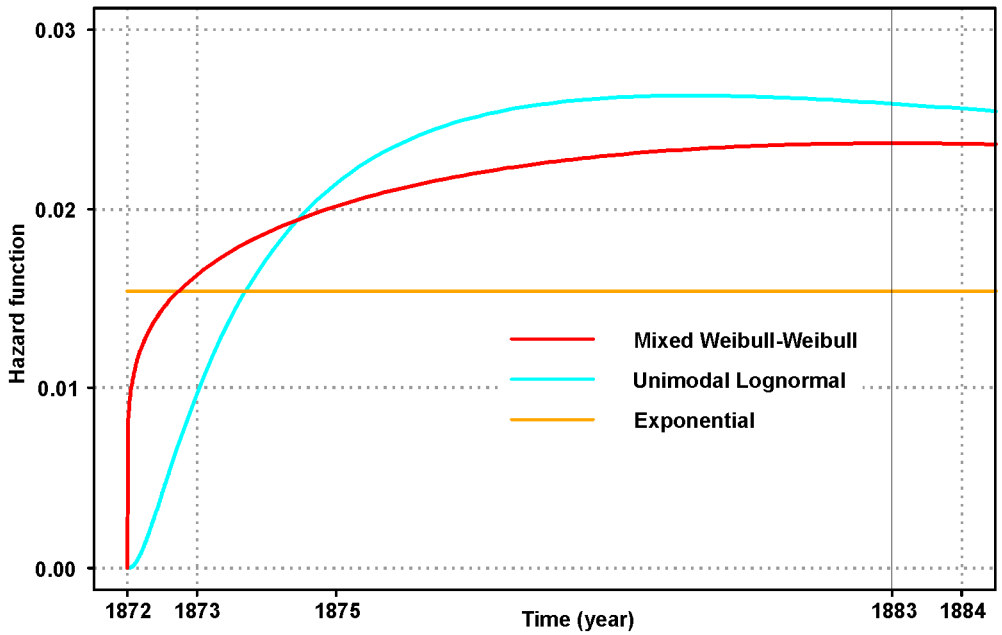

Figure 27. Same as Figure 22 but using the whole data set.

Deutsches GeoForschungsZentrum GFZ
Scientific Technical Report 09/09
DOI:10.2312/GFZ.b103-09098

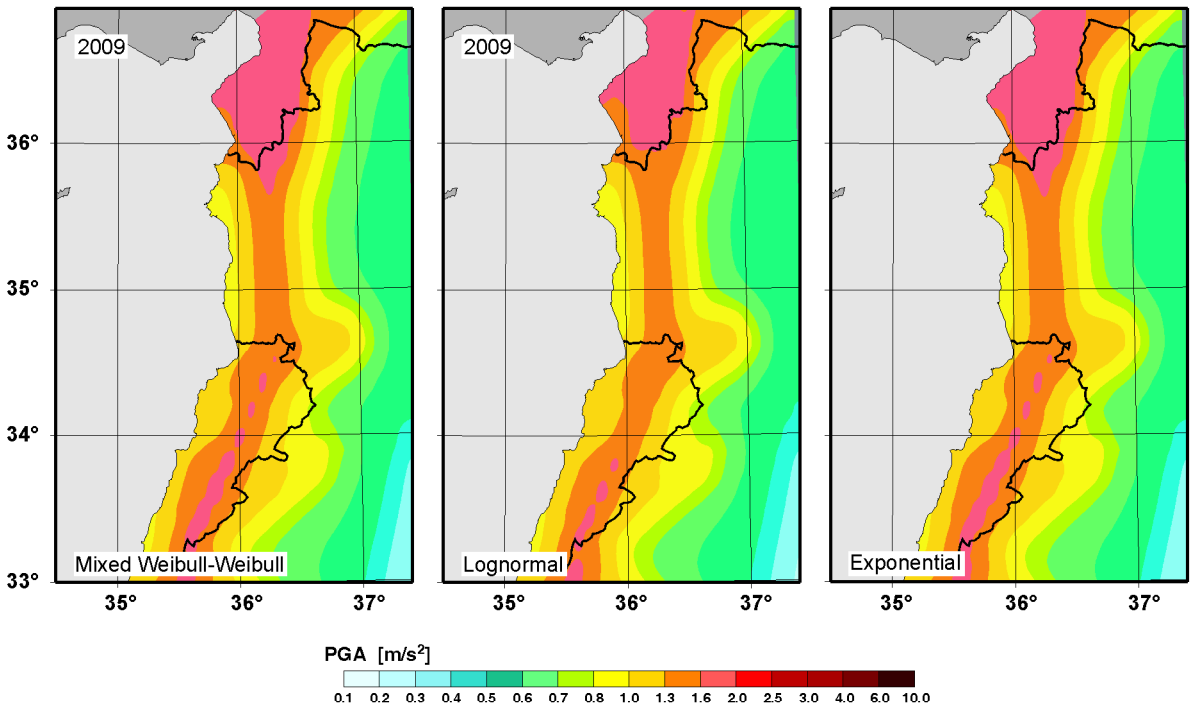

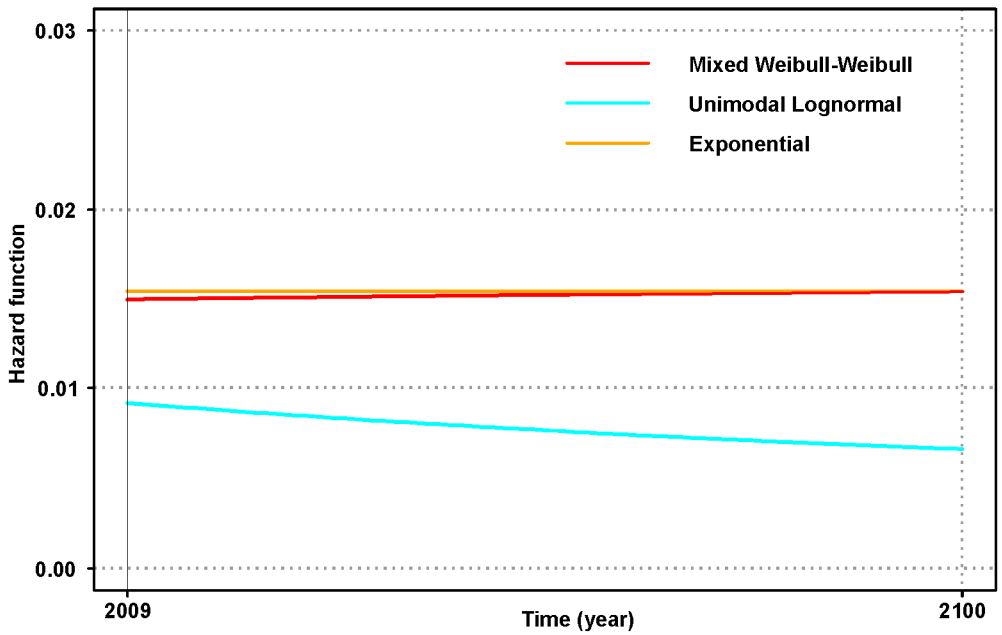

Figure 28. Same as Figure 23 but using the whole data set.

Deutsches GeoForschungsZentrum GFZ
Scientific Technical Report 09/09
DOI:10.2312/GFZ.b103-09098

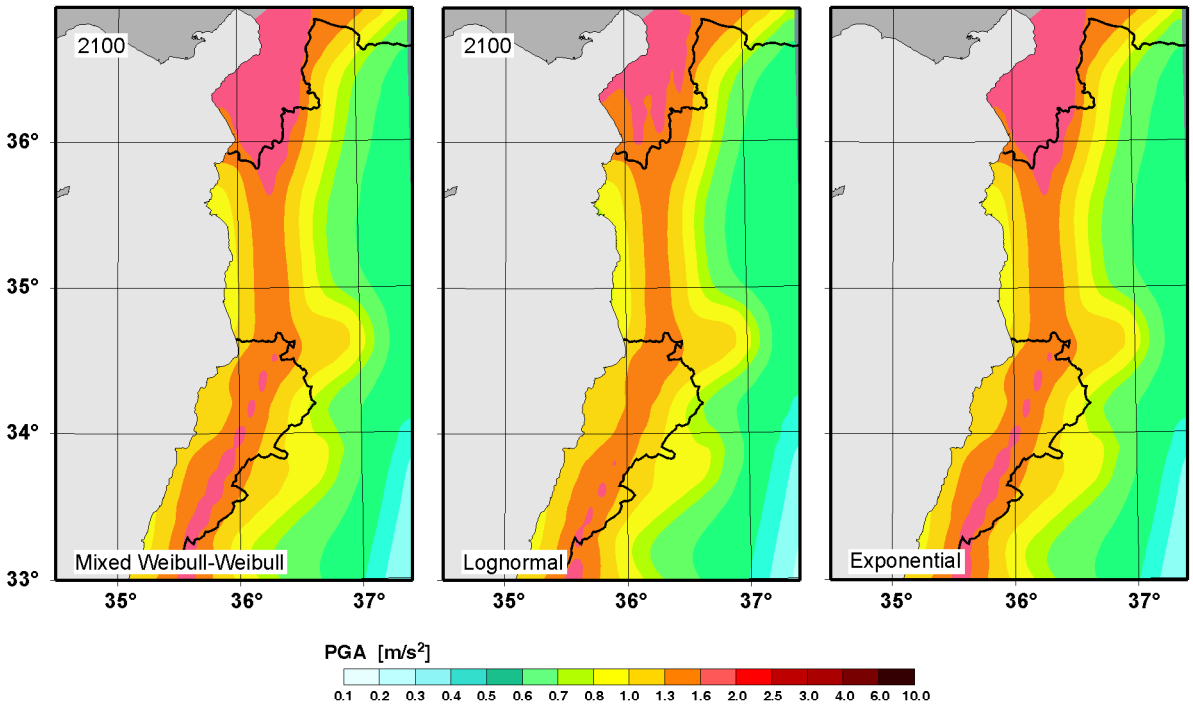

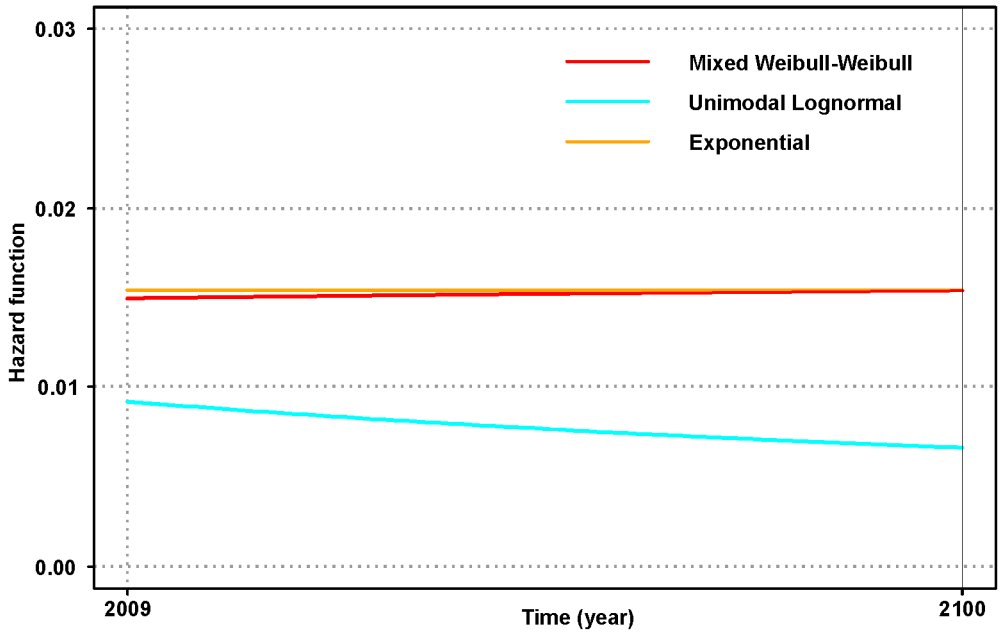

Figure 29. Same as Figure 24 but using the whole data set.

Deutsches GeoForschungsZentrum GFZ
Scientific Technical Report 09/09
DOI:10.2312/GFZ.b103-09098

The hazard maps for the northern part of the DSFZ in the year 1873 (one year after the last large earthquake) show that the seismic hazard based on the mixed Weibull-Weibull distribution is larger than the seismic hazard calculated by the Lognormal model and the exponential (time-independent under Poisson process) distribution. In the year 1875, the seismic hazard based on the mixed Weibull-Weibull distribution is between the seismic hazard based on the Lognormal and based on the exponential distribution. In the year 1883 (about 11 years after the last large event), the seismic hazard based on the mixed Weibull-Weibull distribution is much larger than the seismic hazard based on the exponential distribution, but still less than the seismic hazard based on the Lognormal distribution. In the year 2009 (current time, 137 years after the last large earthquake), the seismic hazard based on the mixed Weibull-Weibull distribution is slightly less than the seismic hazard based on the exponential distribution, while the seismic hazard based on the Lognormal distribution is much lower. Assuming that there will be no earthquake up to year 2100, the seismic hazard based on the mixed Weibull-Weibull distribution is almost equal to the seismic hazard based on the exponential distribution, whereas the seismic hazard based on the Lognormal distribution is extremely low. Finally, it can be concluded that also the hazard maps for the northern part of the DSFZ for each considered year show considerable differences when calculated based on the three different distributions.

Figures 25–29 represent the hazard maps produced for the entire DSFZ using the mixed Weibull-Weibull, the Lognormal, and the classical time-independent (Poisson process) models. The maps are prepared for the same years after the last $M_w \geq 6$ earthquake in the northern part of the DSFZ.

6. Conclusions

The newly developed seismicity data for the study area in terms of harmonized M_w in combination with new GMPE enabled to develop a new generation of PSHA for the Levant as target area, using time-independent as well as time-dependent approaches. None of the so far existing seismicity databases turned out to be sufficiently reliable for a well constrained PSHA for the Levant. Moreover, a considerable number of events in other datafiles turned out to be fake. The derived M_w values for the historical and the instrumental part of the catalogue seem to be more realistic than previous attempts.

The study area for performing a PSHA for the Levant has to encompass the entire Sinai block and the southwestern part of the EAFZ. Based on numerous previous studies, a tectonic model could be derived, which presents the Sinai block in a now better constrained form. This model in combination with further tectonic information and the observed seismicity features were the basis to derive a model of seismic source zones. It consists of four large scale source zones which are subdivided into a set of small scale seismic source zones. The latter have been used for the PSHA, while the b-values of the large scale zones are used in such cases, where the number of events in a small zone is

Deutsches GeoForschungsZentrum GFZ
Scientific Technical Report 09/09
DOI:10.2312/GFZ.b103-09098

too low for a reliable statistical evaluation.

The derived frequency-magnitude relations show surprisingly low scatter and very reasonable *b*-values not only for the large scale source zones. This is no prove of a reached degree of harmonization within the newly derived seismicity database, but a strong indication. The well established frequency-magnitude relations are an excellent basis for a reliable PSHA.

Three GMPE have been selected according to the specific seismotectonic conditions of the target area of the PSHA. The calculated PGA according to this study can be compared with nine other seismic hazard analyses published during the last ten years. A comparison is possible at least at two sites, where the results spatially overlap. Although larger ground motions are usually expected in modern PSHA approaches (*Bommer & Abrahamson* 2006), the opposite is the case with respect to the new study. To some extent, this is probably due to the new harmonized earthquake catalogue we could make use of.

Since the time-independent PSHA is here used for comparisons, not only with previous time-independent approaches, which provide mean values of ground motions, but also with the time-dependent approach, which also could be calculated in terms of best estimates so far, i.e. mean values, there was no need to consider the full range of uncertainties in all the input of the classical PSHA approach, especially the epistemic ones, which enable to provide the results in form of fractiles. These uncertainties will be considered in a follow-up study.

In the northern part of the DSFZ, the inter-event times show a clustering property. The results of applying the method to the inter-event times in this area show a very explicit time dependency for the earthquake occurrence rate. A mixed Weibull-Weibull model has been selected as the best model in this area. This model produces a very high KS-test *p*-value (more than 0.97) and its BIC is relative low. Its statistical hazard function (occurrence rate) increases in the long-term. The hazard function corresponding to the mixed Weibull-Weibull distribution reveals two clusters for the earthquake occurrence rate within the time after an earthquake occurrence. The first cluster begins immediately after an earthquake occurrence and is explicitly time-dependent. This cluster lasts about 80 years. The second cluster begins 80 years after an earthquake occurrence and lasts until the next earthquake occurs. The PSHA corresponding to the latter cluster increases very slowly with time, such that it can be considered, approximately, as a classical time-independent PSHA (based on the Poisson process).

The following can be concluded for this area:

- The PSHA is significantly time-dependent.
- The mixed Weibull-Weibull distribution models the earthquake occurrence rate better than other candidate distributions, because the two different components of the model fit the two different clusters of the inter-event times better than unimodal models.
- Considering the mixed Weibull-Weibull model, the seismic hazard is considerably lower than the time-independent rate immediately after an earthquake, but in-

Deutsches GeoForschungsZentrum GFZ
Scientific Technical Report 09/09
DOI:10.2312/GFZ.b103-09098

creases strongly during the following ten years to reach its maximum, and then decreases over the next 70 years to its minimum which is not much lower than the classical time-independent PSHA.
- More than 80 years after an earthquake, the PSHA increases extremely slowly, so that it can be considered as a time-independent PSHA.

Acknowledgement

We are grateful to all colleagues who have provided data for this study and with whom we have had fruitful discussions during the DFG-funded international project GeoDESIRE. Our thanks are due to S. Strutzke, A.-D. Wirth and U. Lemgo from our research section, who contributed in various steps of this analysis.

Deutsches GeoForschungsZentrum GFZ
Scientific Technical Report 09/09
DOI:10.2312/GFZ.b103-09098

References

Abdallah, A.-Q.A. & the RELEMR Barcelona Working Group: Cooperation in Seismic Hazard Mapping of the Dead Sea Rift Region, Executive Summary. Barcelona, 29 pp., 2006.

Abdallah, A.-Q.A., Feldman, L. & Shapira, A.: The Unified Earthquake Catalogue of the region. Geophysical Institute of Israel, 2004.

Akkar, S. & Bommer, J.J.: Prediction of elastic displacement response spectra in Europe and the Middle East. Earthquake Engineering and Structural Dynamics 36 (10), 1275-1301, 2007.

Akyuz, S.H., Altunel, E., Karabacak, V. & Yalciner, C.C.: Historical earthquake activity of the northern part of the Dead Sea Fault Zone, southern Turkey. Tectonophysics 426 (3-4), 281-293, 2006.

Al-Tarazi, E.: Regional seismic hazard study of the eastern Mediterranean (Trans-Jordan, Levant and Antakia) and Sinai region. Journal of African Earth Sciences 28 (3), 743-750, 1999.

Al-Tarazi, E.: Data base for Jordan Rift Valley and surrounding area. Earth & Environmental Sciences, Inst. of Land, Water, and Environment, Zarqa, Jordan, 2002.

Al-Tarazi, E. & Sandvol, E.: Alternative Models of Seismic Hazard Evaluation along the Jordan–Dead Sea. Earthquake Spectra 23 (1), 1–19, 2007.

Al-Tarazi, E., Sandvol, E. & Gomez, F.: The February 11, 2004 Dead Sea earthquake M_L=5.2 in Jordan and its tectonic implication. Tectonophysics 422 (1-4), 149–158, 2006.

Ambraseys, N.N.: Comparison of frequency of occurrence of earthquakes with slip rates from long-term seismicity data: the cases of Gulf of Corinth, Sea of Marmara and Dead Sea Fault Zone. Geophysical Journal International 165 (2), 516–526, 2006.

Ambraseys, N.N. & Adams, R.D.: Seismicity of the Cyprus region. Terra Nova 5 (1), 85-94, 1993.

Ambraseys, N.N., Simpson, K.A. & Bommer, J.J.: Prediction of horizontal response spectra in Europe. Earthquake Engineering and Structural Dynamics 25 (4), 371-400, 1996.

Ambraseys, N.N., Douglas, J., Sarma, S.K. & Smit, P.M.: Equations for the Estimation of Strong Ground Motions from Shallow Crustal Earthquake Using Data from Europe and the Middle East: Horizontal Peak Ground Acceleration and Spectral Acceleration. Bulletin of Earthquake Engineering 3 (1), 1-53, 2005.

Ambraseys, N.N., Jackson, J.A. & Melville, C.P.: Historical seismicity and tectonics: The case of eastern Mediterranean and Middle East. In: Lee, W.H.K., Kanamori, H., Jennings, J.C. & Kisslinger, C. (eds): International Handbook of Earthquake and Engineering Seismology, Part A, Academic Press, San Diego, 747-763, 2002.

Ambraseys, N.N., Melville, C.P. & Adams, R.D.: The Seismicity of Egypt, Arabia and the Red Sea. Cambridge University Press, 181 pp., 1994.

Arieh, E. & Rabinowitz, N.: Probabilistic assessment of earthquake hazard in Israel. Tectonophysics 161 (3-4), 223-233, 1989.

Deutsches GeoForschungsZentrum GFZ
Scientific Technical Report 09/09
DOI:10.2312/GFZ.b103-09098

Avni, R., Bowman, D., Shapira, A. & Nur, A.: Erroneous interpretation of historical documents related to the epicentre of the 1927 Jericho earthquake in the Holy Land. Journal of Seismology 6 (4), 469–476, 2002.

Bandel, K. & Khouri, H.: Lithostratigraphy of the Triassic of Jordan. Facies 4 (1), 1-23, 1981.

Barazangi, M.: A summary of the seismotectonics of the Arabia region. In: Assessment and Mitigation of Earthquake Risk in the Arab Region, Cidlinsky, K. & Rouhab B. (eds.): Ass. Mit. Earthq. Ris. Arab Reg., UNESCO, 43-58, 1983.

Bommer, J.J. & Abrahamson, N.A.: Why Do Modern Probabilistic Seismic-Hazard Analyses Often Lead to Increased Hazard Estimates? Bulletin of the Seismological Society of America 96 (6), 1967–1977, 2006.

Bommer, J.J., Douglas, J. & Strasser, F.O.: Style-of-Faulting in Ground-Motion Prediction Equations. Bulletin of Earthquake Engineering 1 (2), 171-203, 2003.

Boore, D.M., Joyner, W.B. & Fumal, T.E.: Equations for estimating horizontal response spectra and peak acceleration from western North American earthquakes: A summary of recent work. Seismological Research Letters 68 (1), 128-153, 1997.

Burkhard, M. & Grünthal, G.: Seismic source zone characterization for the seismic hazard assessment project PEGASOS by the Expert Group 2 (EG 1b). Swiss Journal of Geosciences 102 (1), 149-188, 2009.

Cornell, C.A.: Engineering Seismic Risk Analysis. Bulletin of the Seismological Society of America 58 (5), 1583-1606, 1968.

Cornell, C.A.: Probabilistic analysis of damage to structures under seismic loads. In: Dynamic Waves in Civil Engineering, D.A. Howells, I.P. Haigh & C. Taylor (eds.), John Wiley & Sons, New York, 473-488, 1971.

Daëron, M., Klinger, Y., Tapponnier, P., Elias, A., Jacques, E. & Sursock, A.: 12,000-Year-Long Record of 10 to 13 Paleoearthquakes on the Yammoûneh Fault, Levant System, Lebanon. Bulletin of the Seismological Society of America 97 (3), 749-771, 2007.

Diener, C.: Libanon. Grundlinien der physischen Geographie und Geologie von Mittel-Syrien. Alfred Hölder Verlag, Wien, 412 pp., 1886.

Efron, B. & Tibshirani, R.: An introduction to the bootstrap. Chapman & Hall, New York, 1993.

Elnashai, A.S.-E. & El-Khoury, R.: Earthquake Hazard in Lebanon. Imperial College Press, London, 2004.

ETH and Swiss Seismological Service: Data file for Turkey-GSHAP. Swiss Seismological Service, Zurich, Switzerland, 2000. (www.seismo.ethz.ch/gshap/turkey/seisgshap.prn)

Feldman, L. & Amrat, A.-Q.: Database of historical earthquakes. GII Israel and NRA Jordan, 2007.

Freund, R.: A model for the development of Israel and adjacent areas since the Upper Cretaceous time. Geological Magazine 102, 189-205, 1965.

Freund, R., Garfunkel, Z., Zak, I., Goldberg, M., Weissbrod, T. & Derin, B.: The shear along the Dead Sea rift. Philosophical Transactions of the Royal Society of London, Series A: Mathematical and Physical Sciences 267, 107-130, 1970.

Deutsches GeoForschungsZentrum GFZ
Scientific Technical Report 09/09
DOI:10.2312/GFZ.b103-09098

Galanopoulos, A.G. & Delibasis, N.D.: Seismic activity in the Cyprus area. Praktika, Academy of Athens 40, 386-405, 1965.

Garfunkel, Z. & Ben-Avraham, Z.: The structure of the Dead Sea basin. Tectonophysics 266 (1-4), 155-176, 1996.

Garfunkel, Z., Zak, I. & Freund, R.: Active faulting in the Dead Sea rift. Tectonophysics 80 (1-4), 1-26, 1981.

Grünthal, G.: The up-dated earthquake catalogue for the German Democratic Republic and adjacent areas - statistical data characteristics and conclusions for hazard assessment. 3rd International Symposium on the Analysis of Seismicity and Seismic Risk (Liblice/Czechoslovakia), Proceedings Vol. I, 19-25, 1985.

Grünthal, G., Wahlström, R.: A harmonized seismicity data base for the Euro-Mediterranean region. In: Cahiers du Centre Européen de Géodynamique et de Séismologie, Proceedings of the 27th ECGS Workshop "Seismicity Patterns in the Euro-Med Region", Luxembourg, 2009.

Grünthal, G., Bosse, C. & Stromeyer, D.: Die neue Generation der probabilistischen seismischen Gefährdungseinschätzung der Bundesrepublik Deutschland: Version 2007 mit Anwendung für die Erdbeben-Lastfälle der DIN 19700:2004-07 'Stauanlagen'. Scientific Technical Report STR 09/07, Deutsches GeoForschungsZentrum, Potsdam, 81 pp., 2009.

Grünthal, G., Wahlström, R. & Stromeyer, D.: The unified catalogue of earthquakes in central, northern, and northwestern Europe (CENEC) - updated and expanded to the last millennium. Journal of Seismology 13 (4): 517-541, 2009.

Grünthal, G. & GSHAP Region 3 Working Group: Seismic hazard assessment for central, north and northwest Europe: GSHAP Region 3. Annali di Geofisica 42 (6): 999-1011, 1999.

Guidoboni, E. & Comastri, A.: Catalogue of earthquakes and tsunamis in the Mediterranean area from the 11th to the 15th century. Istituto Nazionale di Geofisica e Vulcanologia, 1037 pp., 2005.

Gutenberg, B. & Richter, C.F.: Seismicity of the Earth, Princeton University Press, Princeton, N. J., 310 pp., 1954.

Hakimhashemi, A.: Time-dependent occurrence rates of large earthquakes in the Dead Sea fault zone and applications to probabilistic seismic hazard assessments. PhD Thesis, Potsdam University, 2009.

Harajli, M., Sadek, S. & Asbahan, R.: Evaluation of the seismic hazard of Lebanon. Journal of Seismology 6, 257–277, 2002.

Heidbach, O. & Ben-Avraham, Z.: Stress evolution and seismic hazard of the Dead Sea Fault System. Earth and Planetary Science Letters 257 (1-2), 299-312, 2007.

Hofstetter, A.: Seismic observations of the 22/11/1995 Gulf of Aqaba earthquake sequence. Tectonophysics 369 (1-2), 21-36, 2003.

Hofstetter, R., Klinger, Y., Amrat, A.-Q., Rivera, L. & Dorbath, L.: Stress tensor and focal mechanisms along the Dead Sea fault and related structural elements based on seismological data. Tectonophysics 429 (3-4), 165-181, 2007.

Husein Malkawi, A.I., Al-Homoud, A.S. & Liang, R.Y.: Seismic hazard mapping of Jordan. Quarterly Journal of Engineering Geology 28 (1), 75-81, 1995.

Jiménez, M., Al-Nimry, H., Khasawneh, A., Al-Hadid, T. & Kahhaleh, K.: Assessment of Seismic Hazard in Jordan. First European Conference on Earthquake Engineering and Seismology, Geneva, Switzerland, 3-8 September 2006, paper No. 226, Abstract book, p. 150, 2006.

Kandilli Observatory: Data file of Turkish earthquakes. Kandilli Observatory, Istanbul, Turkey, 2009. (http://www.koeri.boun.edu.tr/sismo/Mudim/katalog.asp)

Khair, K., Karakaisis, G.F. & Papadimitriou, E.E.: Seismic zonation of the Dead Sea Transform Fault area. Annali di Geofisica 43 (1), 61-79, 2000.

Klinger, Y., Rivera, L., Haessler, H. & Maurin, J.-C.: Active Faulting in the Gulf of Aqaba: New Knowledge from the M_w 7.3 Earthquake of 22 November 1995. Bulletin of the Seismological Society 89 (4), 1025-1036, 1999.

Mahmoud, S., Reilinger, R., McClusky, S., Vernant, P. & Tealeb, A.: GPS evidence for northward motion of the Sinai Block: Implications for E. Mediterranean tectonics. Earth and Planetary Letters 238 (1-2), 217-224, 2005.

McGuire, R.: FORTRAN computer program for seismic risk analysis. Open-File Report 76-67, United States Department of the Interior Geological Survey, 1976.

Meghraoui, M., Gomez, F., Sbeinati, R., Van der Woerd, J., Mouty, M., Darkal, A.N., Radwan, Y., Layyous, I., Al Najjar, H., Darawcheh, R., Hihazi, F., Al-Ghazzi, R. & Barazangi, M.: Evidence for 830 years of seismic quiescence from palaeoseismology, archaeoseismology, and historical seismicity along the Dead Sea fault in Syria. Earth and Planetary Science Letters 210 (1-2), 35-52, 2003.

Nemer, T. & Meghraoui, M.: Evidence of coseismic ruptures along the Roum fault (Lebanon): a possible source for the AD 1837 earthquake. Journal of Structural Geology 28 (8), 1379-1568, 2006.

Pankow, K.L. & Pechmann, J.C: The SEA99 Ground Motion Prediction Relations for Extensional Tectonic Regimes: Revisions and a New Peak Ground Velocity Relation. Bulletin of the Seismological Society of America 94 (1), 341-348, 2004.

Pankow, K.L. & Pechmann, J.C.: Erratum: The SEA99 ground-motion predictive relations for extensional tectonic regimes: Revisions and a new peak ground velocity relation. Bulletin of the Seismological Society of America 96 (1), 364-348, 2006.

Papazachos, B.C. & Papaioannou, Ch.A.: Lithospheric boundaries and plate motions in the Cyprus area. Tectonophysics 308 (1-2), 193-204, 1999.

Papazachos, B.C., Comninakis, P.E., Karakaisis, G.F., Karakostas, B.G., Papaioannou, Ch.A., Papazachos, C.B., Scordilis, E.M.: A catalogue of earthquakes in Greece and surrounding area for the period 550BC-1999. In: International Handbook of Earthquake and Engineering Seismology IASPEI, Lee, W.H.K., Kanamori, H., Jennings, P.C., Kisslinger, C. (eds), Part B, CD #3, Academic Press, 2003.

Quennel, A.M.: Tectonics of the Dead Sea rift. 20th International Geological Congress Assoc. Serv. Geol. Afr., 385-405, 1959.

Risk Engineering Ltd.: FRISK88Mc Users Manual, updated version 1.70, 1997.

Deutsches GeoForschungsZentrum GFZ
Scientific Technical Report 09/09
DOI:10.2312/GFZ.b103-09098

Salamon, A., Hofstetter, A., Garfunkel, Z. & Ron, H.: Seismicity of the eastern Mediterranean region: Perspective from the Sinai subplate. Tectonophysics 263 (1-4), 293-305, 1996.

Salamon, A., Hofstetter, A., Garfunkel, Z. & Ron, H.: Seismotectonics of the Sinai subplate – the eastern Mediterranean region. Geophysical Journal International 155 (1), 149-173, 2003.

Sbeinati, M.R., Darawcheh, R. & Mouty, M.: The historical earthquakes of Syria: an analysis of large and moderate earthquakes from 1365 BC to 1900 AD. Annali di Geophysica 48 (3), 347-435, 2005.

Sieberg, A.: Erdbebengeographie. In: Handbuch der Geophysik, Gutenberg, B. (ed.), Verlag Gebrüder Borntträger, Berlin, Band IV, 687-1005, 1932a.

Sieberg, A.: Untersuchungen über Erdbeben und Bruchschollenbau im östlichen Mittelmeergebiet. Jena, G. Fischer, 161-273, 1932b.

Spudich, P., Joyner, W.B., Lindh, A.G., Boore, D.M., Margaris, B.M. & Fletcher, J.B.: SEA99: A Revised Ground Motion Prediction Relation for Use in Extension Tectonic Regimes. Bulletin of the Seismological Society of America 89 (5), 1156-1170, 1999.

Suckale, J. & Grünthal, G.: A probabilistic seismic hazard model for Vanuatu. Bulletin of the Seismological Society of America 99(4): 2108-2126, 2009.

Taylor, H.M. & Karlin, S.: An Introduction To Stochastic Modeling. Third Edition, Academic Press, London, 631 pp., 1998.

Weichert, D.H.: Estimation of the earthquake recurrence parameters for unequal observations periods for different magnitudes. Bulletin of the Seismological Society of America 70 (4), 1337-1346, 1980.

Wells, D.L. & Coppersmith, K.J.: New empirical relationships among magnitude, rupture length, rupture width, rupture area, and surface displacement. Bulletin of the Seismological Society of America 84(4), 974-1002, 1994.

ISSN 1610-0956

Deutsches GeoForschungsZentrum GFZ
Scientific Technical Report 09/09
DOI:10.2312/GFZ.b103-09098